J. Fluid Mech. (1991), *vol.* 226, *pp.* 91–123
Printed in Great Britain

Turbulence in a separated boundary layer

By M. DIANAT† AND IAN P. CASTRO
Department of Mechanical Engineering, University of Surrey, Guildford, Surrey GU2 5XH, UK

(Received 16 May 1990)

This paper presents and discusses the results of an extensive experimental investigation of a flat-plate turbulent boundary subjected to an adverse pressure gradient sufficiently strong to lead to the formation of a large separated region. The pressure gradient was produced by applying strong suction through a porous cylinder fitted with a rear flap and mounted above the boundary layer and with its axis in the spanwise direction. Attention is concentrated on the structure of the turbulent flow within the separated region and it is shown that many features are similar to those that occur in separated regions produced in a very dissimilar manner. These include the fact that structure parameters, like Reynolds stress ratios, respond markedly to the re-entrainment of turbulent fluid transported upstream from the reattachment region, the absence of any logarithmic region in the thin wall boundary layer beneath the recirculation zone and the lack of any effective viscous scaling in this wall region, and the presence of a significant low-frequency motion having timescales much longer than those of the large-eddy structures around reattachment.

Similarities with boundary layers separating under the action of much weaker pressure gradients are also found, despite the fact that the nature of the flow around separation is quite different. These similarities and also some noticeable differences are discussed in the paper, which concludes with some inferences concerning the application of turbulence models to separated flows.

1. Introduction

There have been many studies of boundary-layer separation and reattachment, but detailed measurements of turbulence quantities within the separated flow itself are still very rare, at least in cases where the surface is not discontinuous. However, in the context of flows in which separation is fixed by the geometry – as in backward-facing steps or normal flat plates with splitter plates, for example – there are rather more data available and it has become clear that the structure of such flows differs in many important respects from that of more classical shear flows. Studies in our laboratory have shown, for example, that in the shear layer bounding the separated flow region behind a flat plate normal to the oncoming flow and fitted with a central splitter plate the changes in Reynolds stresses are large and differ for each stress component. The stabilizing curvature present almost all the way to reattachment is not the dominating influence on the mixing layer, which is manifestly *not* like a curved version of the classical plane mixing layer. Changes in the turbulence structure seem to be dominated by the re-entrainment of turbulent fluid returned upstream around reattachment, which provides a kind of 'positive feedback' of

† Present address: Safety Modelling Division, Midlands Research Station, British Gas plc, Solihull, UK.

energy to the separated shear layer and is limited only by the presence of the wall (see Castro & Haque 1987, 1988 for fuller discussion).

Further, longitudinal velocity autocorrelation data obtained within this separated flow imply a behaviour consistent with that commonly observed in different but related geometries (Eaton & Johnston 1982; Cherry, Hillier & Latour 1984; Kiya & Sasaki 1983 and Castro 1981). There is a low-frequency motion of the whole flow on a timescale much longer than that associated with the usual large-eddy motions in the mixing layer. As a third example of apparently common features in such flows, it has been found that the flow close to the wall within the recirculating region has features reminiscent of an (albeit very unsteady) laminar boundary layer. This is not to say that it *is* an unsteady laminar boundary layer – collapse of mean velocity profiles using viscous wall units alone is not possible – but the usual semi-logarithmic profile certainly does not exist and a laminar-like collapse of the wall friction with Reynolds number seems fairly universal in separated flows of quite different geometry (see Adams & Johnston 1988 for a recent discussion).

In flows where separation occurs from a smooth surface the separation process itself is in many respects quite different from what occurs in cases of sharp-edged separation. Whilst there have been many studies of boundary layers in pressure gradients sufficiently strong to lead to separation, very few workers have undertaken detailed turbulence measurements within the separated flow itself (see Simpson, Chew & Shivaprasad 1981*a*, *b* and Dengel & Fernholz 1990, for some examples). However, the data are sufficiently extensive to demonstrate, amongst other things, that the Reynolds stresses are significantly higher than in attached flows, that the normal stress terms can make an important contribution to turbulence energy production near the wall, that turbulent transport processes are important and cannot be adequately described by gradient diffusion processes, and that there is no semi-logarithmic region in the mean velocity profiles near the wall in the separated zone. Some of these features are present in the separated flows discussed earlier, but there are also some distinct differences. One of the most significant, perhaps, is that although in these latter flows the mean backflow comes at least partly from far downstream (around reattachment), Simpson concluded that in his separated boundary layer this was not the case (see Simpson 1985, for example). However, Simpson's measurements did not extend throughout the whole of the reversed flow region, so that the processes around reattachment and their links with what occurs further upstream were not clarified completely – partly because of the large influence of three-dimensionality in the latter part of the flow.

It is important to clarify to what extent some of the distinguishing features of separated flows, noted above, are dependent on the processes around separation itself. If these processes are of only secondary importance in determining the nature of the bulk of the separated flow, many features of the latter may turn out to be universal – at least for two-dimensional separated flows. This would ease considerably the technical difficulties that arise in attempting to predict such flows. As a step toward such clarification and as part of our ongoing program of work on complex turbulent flows, we have undertaken an extensive study of a separated boundary-layer flow generated using a much stronger adverse pressure gradient than that employed by Simpson. Pulsed-wire anemometry has been used to measure turbulence quantities up to third-order velocity products so that many of the terms occurring in the turbulence energy transport equation as well as the momentum equations could be derived.

Some of the initial mean flow results have already been presented (Castro, Dianat

& Haque 1988; Dianat & Castro 1989); here we summarize these and present a subset of the extensive turbulence data. In view of the somewhat unusual history of the boundary layer prior to separation (see § 4) and the inevitable three-dimensional effects, we do not believe that this flow is particularly suitable as a test case for numerical modellers. It is therefore not appropriate to present all of the data in great detail. However, the results extend the available database for separated flows and, more importantly, have some important implications in terms of clarifying the physics of such flows and it is on that basis that we present this work.

The experimental techniques and the mean flow data are summarized in §§ 2 and 3, respectively. Section 4 presents the major turbulence stress data whilst momentum and turbulence energy balances are discussed in § 5 and timescales in § 6. Some implications for turbulence modelling are given in the final section, along with a summary of the major conclusions.

2. Apparatus and techniques

2.1. *Generation of the separated flow*

All measurements were made in the no. 1 blowdown, open circuit tunnel in the Department of Mechanical Engineering, University of Surrey. Its working section is $0.76 \times 0.61 \times 4$ m long and the maximum velocity is around 17 m/s. The free-stream turbulence level is below 0.25%. To generate the separated flow a method similar to that used by Woodward (1970) to study laminar separation bubbles was used. Chu & Young (1976) found the same method equally effective in producing turbulent separation. The apparatus has been described in detail by Dianat & Castro (1989) and is shown in figure 1. A porous cylinder was mounted through the tunnel sidewalls above a long aluminium flat plate equipped with a number of instrumentation ports. Its axis was about 2.7 m from the plate's leading edge and it was fitted with a small flap at the rear to generate the required circulation on application of suitable suction through the cylinder's porous surface – the flap acts to fix the rearward stagnation point and the suction maintains attached flow. The pressure gradient on the flat surface below was therefore initially favourable and then adverse. To prevent strong three-dimensional effects at the junction between the cylinder and the tunnel sidewalls the cylinder passed through porous discs set into the sidewalls; the same suction pressure was applied to these discs.

The suction required to maintain attached flow around the cylinder was determined by inspection of wool tufts placed both on the cylinder surface and within the downstream flow. After considerable trial and error a flap angle of 50° was finally chosen as one which produced an adequate fully separated boundary layer, the major criteria being the requirement for a separated flow zone sufficiently large to make application of pulsed-wire anemometry viable, whilst being sufficiently small to minimize the inevitable three-dimensional effects arising from the interaction of the separated flow with the tunnel sidewalls. Hot-wire traverses showed that the cylinder wake was very thin and of low turbulence intensity (less than 2% even at two diameters downstream). Oil flow visualization showed that the separation line, which was 80 mm downstream from the point immediately beneath the cylinder axis, was remarkably straight across the whole tunnel span. Fluctuations in the separation position were quite limited and probably simply a result of the high levels of turbulence in the separation region itself; they were certainly not caused by the cylinder flow, which was exceedingly steady. Reattachment occurred 0.85 m

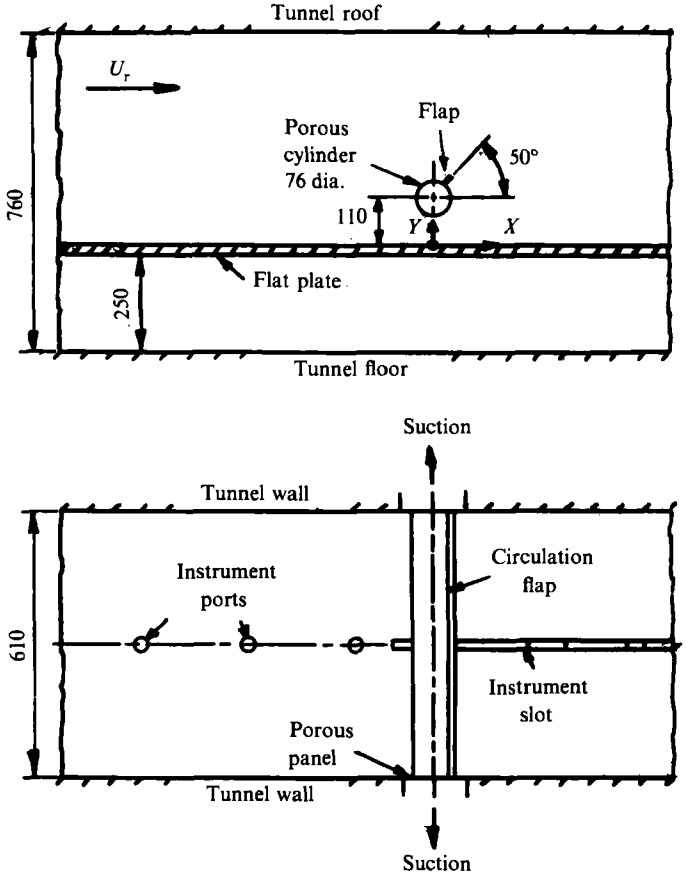

FIGURE 1. Experimental set-up – not to scale. Dimensions in mm.

downstream of separation and the reattachment line was straight (to within $\pm 1.5\%$ of the 'bubble' length) over the central half of the span. Traverses within the separated flow showed that spanwise variations in mean velocity did not exceed about $\pm 1\%$ over the central third of the span, except near the separation line. Here, the surface flow tended to move sideways and outwards, with a weak saddle point close to the spanwise centreline, which was found to be accurately the symmetry axis. Jaroch & Fernholz (1989) have recently discussed the effect of such three-dimensionalities on separated flows. Whilst it is not possible to generate a truly two-dimensional (planar) separated flow, we believe that the dominant mean and turbulent features of the present flow are not qualitatively altered significantly by the three-dimensionality, although its effects are probably large enough to invalidate detailed quantitative comparisons with numerical predictions based on two-dimensional equations. The ratios of tunnel width to boundary-layer thickness and displacement thickness around reattachment were about 2.5 and 6, respectively.

2.2. *Measurement techniques*

Surface static pressures and velocities in regions of low turbulence intensity were obtained using standard pressure transducers and hot-wire anemometry. To obtain fluctuating surface pressures an Endevco high-frequency transducer was used; this

had a frequency response which was flat up to about 1 kHz and was used with a high-gain precision amplifier. As usual for such measurements, extreme care was necessary to eliminate all sources of electronic noise and 'pick-up' from the electrical leads. Background tunnel disturbances (largely attributable to unsteadiness at the fan frequency) led to measurements of fluctuating pressure energies in the zero-pressure-gradient boundary layer well upstream that were somewhat higher than the value found by, for example, Willmarth & Roos (1965). However, this was less of a problem within the separated flow where the fluctuating pressures were inevitably much higher.

For wall friction measurements Preston tubes were used where possible, but for wall friction and mean and fluctuating velocities in the highly turbulent regions pulsed-wire anemometry was used. The latter required a relatively low tunnel speed; the reference velocity, U_r, taken as the free-stream velocity some 2 m upstream of the cylinder, was around 7 m/s. Details of the skin friction probe, which was calibrated against Preston tubes in the upstream boundary layer, are given in Castro, Dianat & Bradbury (1987). The 'through-wall' probe for measurements throughout the sub-layer, and the method used to obtain Reynolds stresses are described in Castro & Dianat (1990) and Castro & Cheun (1982), respectively. Velocity triple-product measurements ($\overline{u^3}$, $\overline{v^3}$, $\overline{u^2v}$ and $\overline{v^2u}$) in separated flows are extremely rare. To our knowledge only Chandrsuda & Bradshaw (1981), using hot wires, and Driver & Seegmiller (1985), using laser-Doppler anemometry, have previously reported any; the former data are inevitably somewhat unreliable. Measurements of velocity triple products in the present case were made using an extension of the methods employed for obtaining the stresses and it is worth outlining our procedures.

In principle, it is a simple matter to obtain data from the pulsed-wire probe rotated at various angles so as to deduce the velocity moments. For the stresses ($\overline{u^2}$, $\overline{v^2}$ and $\overline{uv}$), this requires at least three angles. With the probe at an angle α to the x-axis the relationships between the measured second and third fluctuating velocity moments, $\overline{u_\alpha^2}$ and $\overline{u_\alpha^3}$, and their values at $\alpha = 0$ are

$$\overline{u_\alpha^2} = \overline{u^2}\cos^2\alpha + \overline{v^2}\sin^2\alpha + \overline{uv}\sin 2\alpha, \tag{1a}$$

$$\overline{u_\alpha^3} = \overline{u^3}\cos^3\alpha + \overline{v^3}\sin^3\alpha + 3\overline{u^2v}\sin\alpha\cos^2\alpha + 3\overline{uv^2}\sin^2\alpha\cos\alpha. \tag{1b}$$

It has been shown that, provided the probe geometry is arranged to ensure a particularly good yaw and pitch response, three angles will in fact suffice to give second-order quantities in flows of arbitrarily high intensity with an accuracy at least as good as that obtainable by crossed hot wires in flows where the latter are appropriate (Castro & Cheun 1982; Jaroch 1985). To obtain all four coplanar triple products one requires measurements at four different angles at least. Extensive measurements in a variety of flows convinced us that use of *only* four angles led to quite unacceptable scatter and uncertainty in the resulting triple products. Even taking 10000 velocity samples at each probe angle led to sufficient variability in the measurement of $\overline{u_\alpha^3}$ to make the derivation of the triple products – which often requires subtraction of two large quantities of similar magnitude – very uncertain.

However, it was found that the uncertainties could be considerably reduced by increasing the number of different angles and using a least-squares fitting procedure to deduce the four unknown moments in (1*b*). 10–12 angles in the range $-60° < \alpha < 60°$ were usually used and a screen plot of the resulting values of u_α^3 was produced immediately subsequent to the measurements, so that any points clearly out of line could be rejected prior to performing the least-squares fit. Since the direction of the

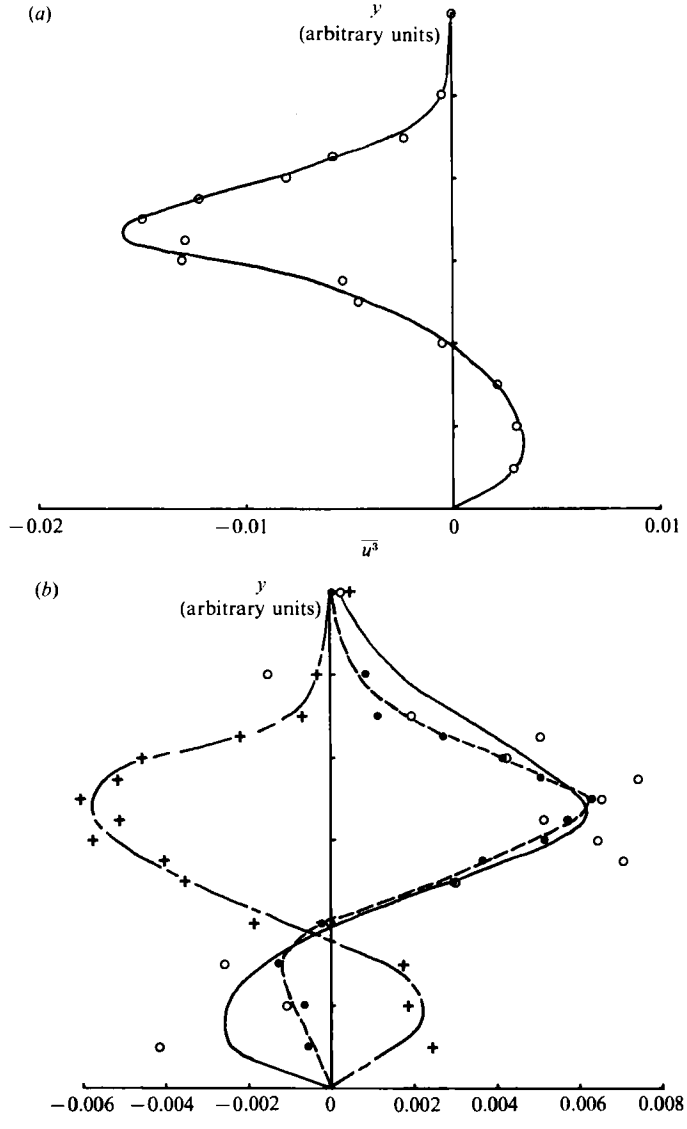

FIGURE 2. Velocity triple products in the separated boundary layer at $x/L_r = 0.77$. (*a*) $\overline{u^3}$; (*b*) ○, $\overline{v^3}$; ●, $\overline{u^2v}$; +, $\overline{v^2u}$. All normalized by U_r^3.

mean velocity vector was not always known *a priori*, bad points could arise when one of the angular positions of the probe led to large numbers of the instantaneous velocity vectors lying outside the angular 'acceptance cone' of the probe.

This whole procedure meant that obtaining adequate data for even one cross-stream profile of triple products was a somewhat lengthy process but, as shown by the typical results in figure 2, the resulting scatter in the final data was generally acceptable. Corresponding profiles at other axial locations within the separated zone generally indicated reasonably smoothly varying x-direction profiles, so the data are at least internally consistent and repeatable. Note that the scatter tends to rise with the power of the lateral velocity component, so that measurements of $\overline{v^3}$ and, to a lesser extent, $\overline{uv^2}$ are somewhat less certain than those of the other two components.

In the worst case scatter about a smooth line drawn through the data points (for $\overline{v^3}$) was generally less than $\pm 30\%$ and considerably lower for the sums of triple products which appear in the turbulence energy equation (see figure 8*b*, for example). Whilst we cannot claim a particularly high level of accuracy for our triple-product measurements, we believe that they are as accurate as can be achieved with any current instrumentation and are also likely to be as accurate as can be achieved with hot-wire anemometry in much lower intensity flows. It is worth pointing out that although the data in figure 2 were obtained *within* the separated region, the levels of scatter are much lower than those evident in the laser-Doppler anemometry results of Simpson and his colleagues, which were confined to the region *upstream* of separation (Simpson *et al.* 1981*b*).

3. The mean flow

Figures 3 and 4 show the centreline variations of mean and fluctuating wall pressure and skin friction, respectively, with the separation and reattachment locations included. C_p is defined by $2(p_s - p_r/\rho U^2$, C_f by $2\tau_w/\rho U^2$ and the fluctuating values similarly, where subscripts s and r refer to local surface static pressure and reference conditions, respectively, and τ_w is the wall shear stress. Reattachment occurred a little way downstream of the last surface instrumentation port so its location was determined using a surface-mounted twin-tube pressure probe. Later velocity profiles were consistent with these measurements. The history of the flow prior to separation is complex; after an initial rapid rise in C_f because of the strong acceleration there is a non-monotonic variation. Preston tube data gave no indication of this and it was only use of the pulsed-wire probe, which does not rely for accuracy on the presence of a logarithmic region, which clearly showed the unexpected response of the flow. It was argued previously (Dianat & Castro 1989) that relaminarization of the boundary layer initially occurs and this laminar layer persists into the adverse pressure gradient region – almost to separation. Transition occurs, however, so C_f rises again, before the continuing deceleration of the flow causes full turbulent separation 80 mm downstream of the cylinder axis (figure 4*a*). Skin friction fluctuation amplitudes are particularly large around transition compared with their values within the separation region, whereas pressure fluctuations are not (compare figures 3*b* and 4*b*), probably because the latter are dominated in the separated region by contributions from a very much wider range of scales than is present in the transition region. Large skin friction fluctuations around transition are consistent with the large (more qualitative) fluctuations often measured with surface hot films used to locate transition.

The separation process is in one sense very much more rapid than that in Simpson's experiment (Simpson *et al.* 1981*a*, *b*), where the distance between the first occurrence of instantaneous backflow near the wall was some 380 mm upstream of the final separation point (defined as the location where the backflow intermittency was 50%). However, if this distance is normalized by an appropriate boundary-layer thickness the distance between the first occurrence of instantaneous backflow at the wall and the mean separation point in the two flows is quite similar.

An estimate of the pressure gradient parameter, $K = (\nu/U_e^2)\,\mathrm{d}U_e/\mathrm{d}x$, where U_e is the local free-stream velocity, indicated that it exceeded by a large margin the value at which the entire boundary layer is prone to relaminarize (3×10^{-6} according to Kays & Crawford 1980). With the present rig it was not possible to reduce this sufficiently to prevent relaminarization without preventing separation altogether. In

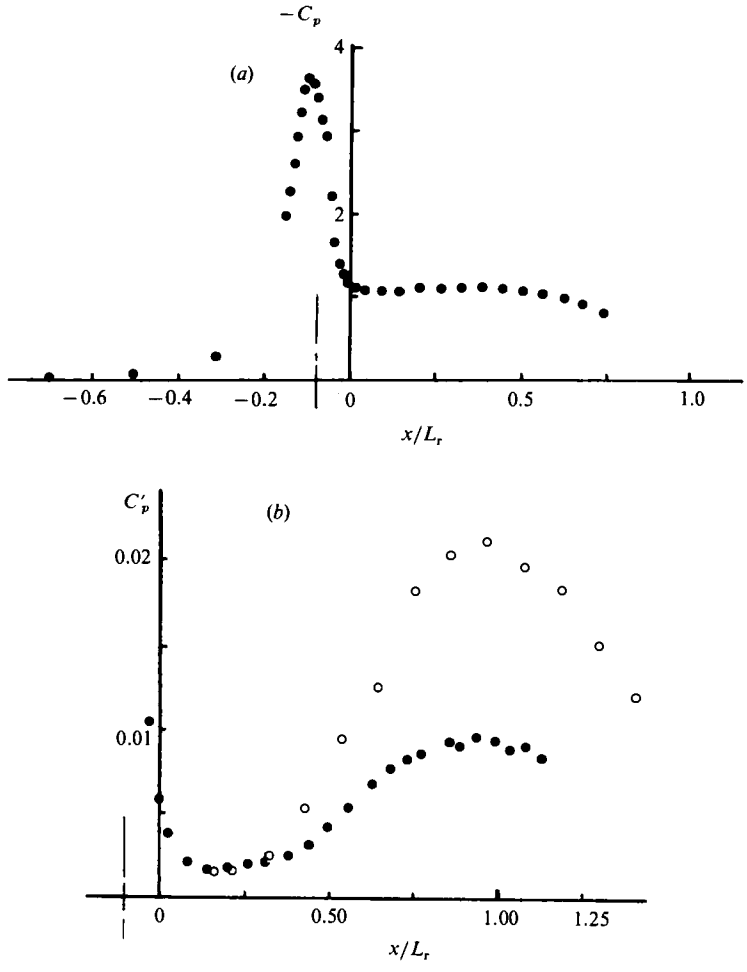

FIGURE 3. (*a*) Mean and (*b*) fluctuating static pressure. —·—, Cylinder axis location. (*b*) ●, Present data; ○, Kiya *et al.* (1982).

Simpson's experiment (Simpson *et al.* 1981*a*, *b*) K was about an order of magnitude lower, so the state of the boundary layer at separation is quite different in the two cases. This is emphasized by the fact that the (laminar) boundary-layer thickness just 80 mm upstream of separation (i.e. directly under the cylinder axis) was about 1.5 mm, less than 3% of its value at the same location but in the absence of the cylinder. In this region just prior to separation mean velocity measurements, obtained using the 'through-wall' pulsed-wire probe, showed the complete absence of any logarithmic region, which emphasizes the inapplicability of Preston tubes. Further details of this part of the flow are given in Dianat & Castro (1989).

Figure 3(*b*) includes the data of Kiya, Sasaki & Arie (1982), obtained in the separated flow at the front of a thick flat plate normal to the oncoming flow. Quantitative levels depend on the normalizing velocity; in the latter case the reference value far upstream was used, whereas for the present data the (maximum) value above the separation point was used. A more appropriate velocity would, perhaps, be $\Delta U_{\max}$, the largest total velocity difference across the separated shear layer, which would lead to a rather closer collapse. In any case, the qualitative

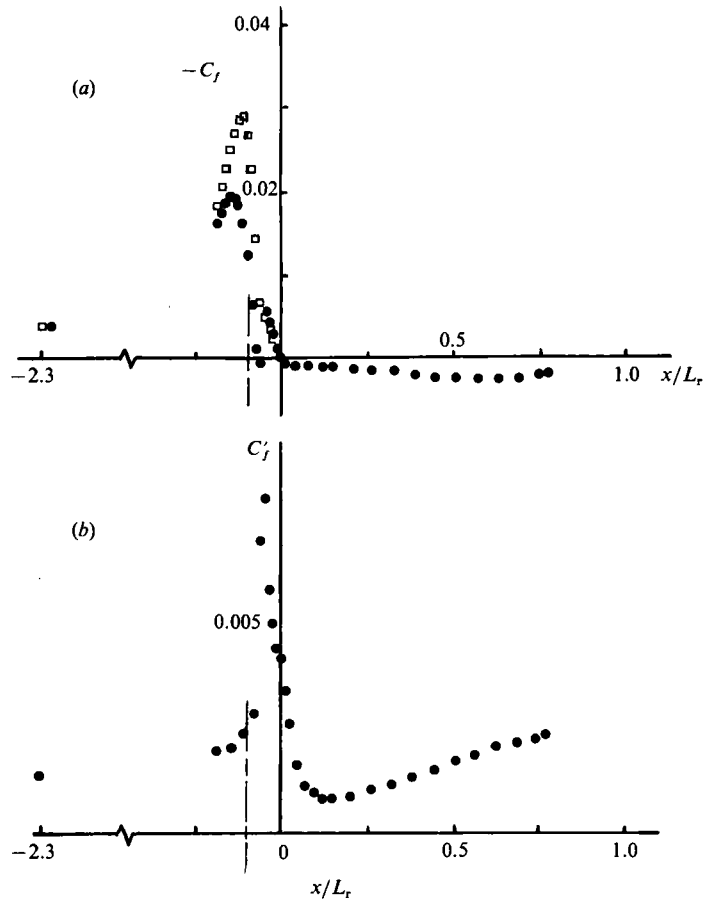

FIGURE 4. (*a*) Mean and (*b*) fluctuating wall friction. □, Preston tube data; —·—, cylinder axis location.

similarity is clear, with the largest pressure fluctuations occurring around reattachment in both cases. This seems a fairly universal feature of separating–reattaching flows.

Figure 5 shows the mean flow streamlines deduced by integrating the comprehensive set of mean flow profiles obtained through the separated flow. Also shown are some locations of maximum temperature in the wake of a heated wire stretched across the tunnel just behind the cylinder. Making the reasonable assumption that these represent points on the mean streamline through the location of the heated wire, the data are closely consistent with streamlines deduced from the pulsed-wire data, and provide an independent test of the accuracy of the latter. The discrepancy between the V-component velocities deduced by solving the continuity equation using the measured U-component data, and those obtained directly from the pulsed-wire data during the course of second- and third-order moment measurements was typically about $\pm 2\%$ of U_r, the free-stream velocity far upstream. This is similar to that found in the case of the normal flat-plate flow (Castro & Haque 1987, hereinafter referred to as CH) and is the same order of accuracy as that expected from crossed hot-wire anemometry in regions where the latter can be sensibly used.

Lines of maximum turbulence energy, zero axial velocity and $\eta = 0$ are also

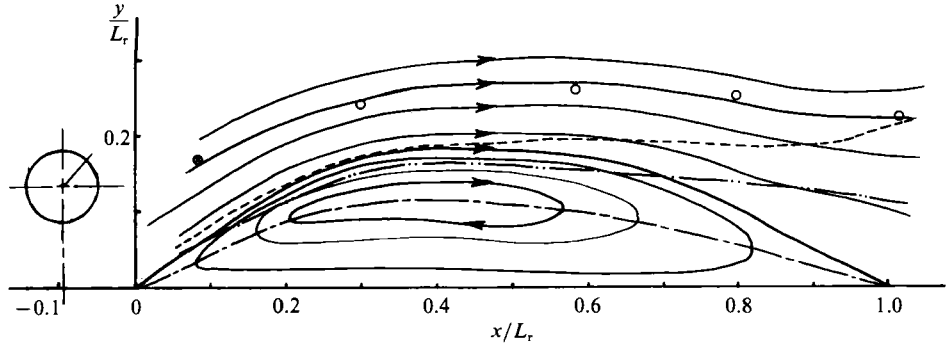

FIGURE 5. Mean flow streamlines (solid lines); ○, from thermal wake; ----, $\eta = 0$; -——-, $U = 0$; —·--—, line of maximum q^2; ⊗, heated wire.

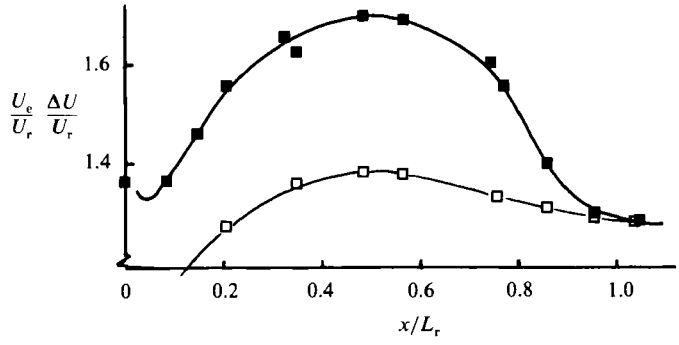

FIGURE 6. Axial variation of the maximum velocity difference across the layer (ΔU, ■) and free-stream velocity at edge of boundary layer (U_e, □).

included in figure 5; these will be discussed later. To be consistent with the ordinary plane mixing layer, for which $\eta = 0$ is often defined as the line $y = 0$ (parallel to the external freestream), η is defined here as $\eta = -(y-y_c)/\Lambda$ where y_c, the nominal shear-layer centreline, is the position at which the mean axial velocity is $(0.67\Delta U + U_N)$. y_c would be zero for a plane mixing layer. U_N is the minimum velocity on the low-speed side of the shear layer (negative for $x < L_r$) and Λ is the vorticity thickness, defined in the usual way by

$$\Lambda = 1/[\mathrm{d}(U/\Delta U)/\mathrm{d}y]_{\max}.$$

x is measured from the separation point and L_r is the distance between $x = 0$ and the mean reattachment point (see CH for brief discussion of these definitions). Figure 6 shows the axial variation of the velocity difference across the layer, $\Delta U = U_e - U_N$, where U_e is the maximum velocity on the high-speed side of the flow.

Figure 7 shows the vorticity thickness, normalized by both L_r (figure 7*a*) and R (figure 7*b*), where R is the radius of curvature of the separating streamline. R was found to be close to constant throughout most of the flow (as in the normal flat-plate case), with a value given by $R/L_r = 0.784$. There is somewhat less evidence of a gradual fall in shear-layer growth rate as reattachment is approached than in the normal flat-plate flow, and it is evident that the growth rate over most of the flow is similar to that for an ordinary plane mixing layer. Λ/R (figure 7*b*) can be thought of as a measure of the possible importance of mean flow curvature effects; values between 0.1 and 0.2 were typical in the curved-mixing-layer experiment of Castro &

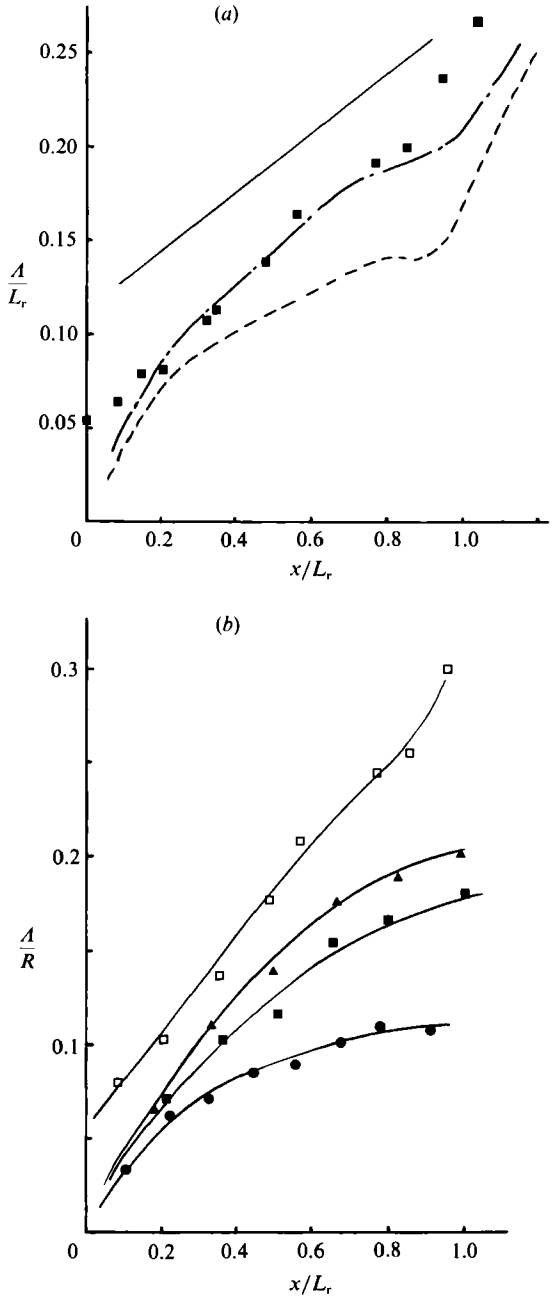

FIGURE 7. Variation of shear-layer thickness, normalized by (*a*) length of the recirculation region or (*b*) curvature of the separation streamline. (*a*) ■, Present data; ----, CH; —·—, CH plus free-stream turbulence (FST) of 8.7% intensity; ——, plane-mixing-layer slope (arbitrary offset). (*b*) □, Present data; ●, CH; ■, CH plus 3.4% FST; ▲, CH plus 8.7% FST.

Bradshaw (1976). It is therefore particularly significant that, although this parameter is everywhere larger in the present flow than in the normal flat-plate flow, the growth rate is also larger (figure 7*a*), being similar to the latter case only when this flow includes significant levels of free-stream turbulence. Now in more classical shear

flows stronger stabilizing curvature inevitably leads, in the absence of other distortions, to reductions in growth rate (and Reynolds stresses). It is therefore clear that mean flow curvature cannot be the only feature which controls the behaviour of the separated boundary layer. This is discussed further in due course.

Mean velocity profiles within the separated region and very close to the wall were presented and discussed by Castro *et al.* (1988). These demonstrate the absence of any logarithmic region within this boundary layer; other data sets are similar in this respect (e.g. Adams, Johnston & Eaton 1984; Simpson *et al.* 1981*a*, *b*) and it seems now to be generally well accepted that such boundary layers, whilst not strictly laminar, do have certain 'laminar-like' features. This does not imply that the velocity in the near-wall region scales solely on viscous wall units; our earlier work show that it does not. Neither do velocity profiles necessarily conform with the model suggested by Simpson (1983). However, Devenport's (1985) generalized form of this model, which takes pressure gradients into account and has no disposable constants, *does* fit our data very well (see Castro *et al.* 1988). What happens at significantly higher Reynolds numbers remains an open question. Using a Reynolds number appropriate to the thin boundary layer itself rather than to the overall external separated flow, all the (very limited) available data have been obtained at Reynolds numbers which are quite low. Presumably, at higher Reynolds numbers the wall boundary layer beneath separated regions takes on the more usual fully turbulent features, but this has yet to be demonstrated. Adams & Johnston (1988) have recently discussed these points in some detail.

4. Reynolds stresses and higher moments

4.1. *Basic data*

Complete profiles of $\overline{u^2}$, $\overline{v^2}$, $\overline{w^2}$, $\overline{uv}$, $\overline{u^2v}$, $\overline{v^2u}$, $\overline{u^3}$ and $\overline{v^3}$ were obtained at $x = 7$, 18, 29, 40, 47, 64, 71, 79 and 87 cm. It would not be appropriate to include plots of all these quantities at every station; instead, figure 8 presents profiles of all the variables at just one station ($x = 47$ cm, $x/L_r = 0.566$). These are typical of profiles at other stations and indicate the general level of experimental scatter in the data. Note that the triple products in figure 8(*b*) are shown as the sum of those which appear together in the turbulence energy equation. Major features of this data, like the maximum value of the Reynolds stresses and the value of the turbulence energy, $\frac{1}{2}\overline{q^2} = \frac{1}{2}(\overline{u^2}+\overline{v^2}+\overline{w^2})$, along with parameters deduced from the mean velocity profiles, like the vorticity thickness, Λ, are given in table 1.

For all subsequent calculations (and in table 1), the turbulence energy ($\frac{1}{2}\overline{q^2}$) was taken as $\frac{3}{4}(\overline{u^2}+\overline{v^2})$, because $\overline{w^2}$ measurements, which have to be obtained with the pulsed-wire probe oriented so that the pulsed wire is in the direction of the velocity shear, were not as detailed as the (u, v)-plane measurements. Figure 9 shows that the energy deduced in this way is close to that obtained by summing all the separately measured stress components. Figure 9 also shows the $\overline{uv}$ and the $\overline{uw}$ stress profiles, demonstrating that the latter is satisfactorily small; in the absence of three-dimensional effects (or at least on a symmetry plane) it should ideally be zero. It is everywhere smaller than $\overline{uv}$ by at least an order of magnitude, which provides some confirmation of the internal consistency of the measurement technique. The inset to figure 9 shows that the near-wall $\overline{uv}$ measurements are consistent with the wall value deduced from the independent skin-friction measurements, although the latter must be Reynolds-number dependent, as discussed by Castro *et al.* (1988).

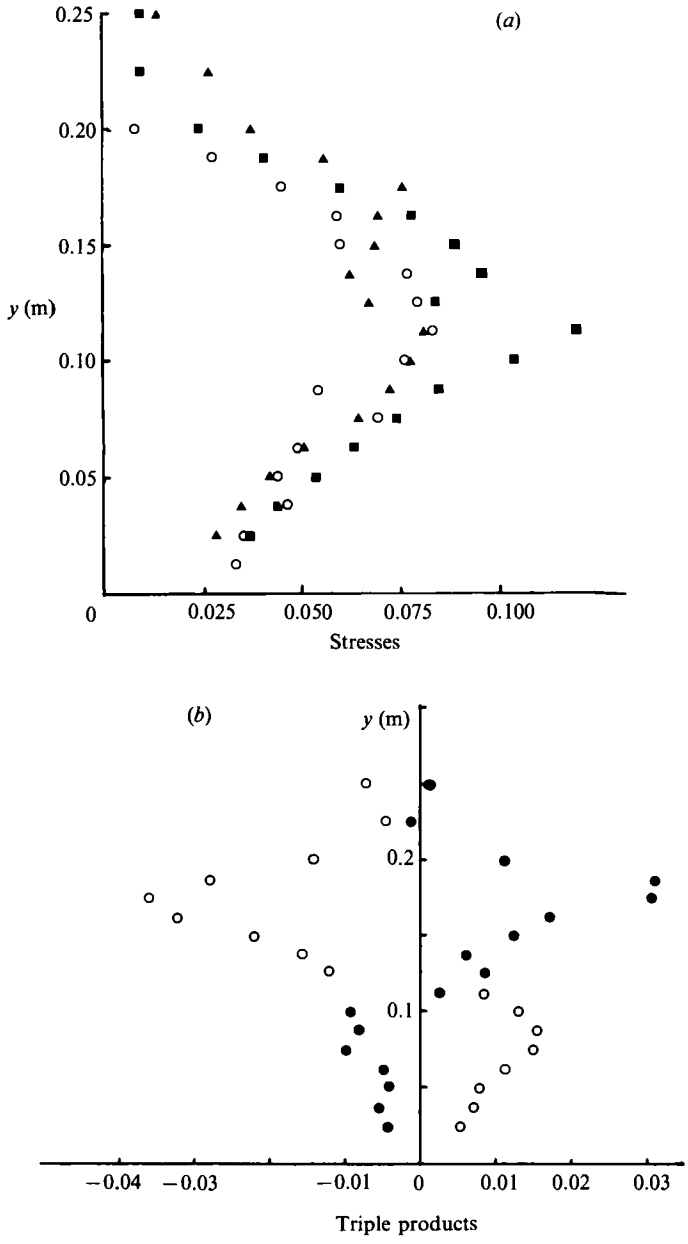

FIGURE 8. Cross-stream profiles at $x = 47$ cm of (*a*) Reynolds stresses and (*b*) triple products. All normalized using U_r. (*a*) ■, $\overline{u^2}$; ▲, $\overline{v^2}$; ○, $\overline{w^2}$. (*b*) ●, $(\overline{v^3}+\overline{u^2v})$; ○, $(\overline{u^3}+\overline{uv^2})$.

4.2. *Derived quantities and discussion*

It is of interest, first, to compare the general level of the Reynolds stresses with those measured by Simpson and his colleagues in a boundary layer separating under a much milder adverse pressure gradient. They state that $\overline{w^2} = \overline{v^2}$ within most of the separated region (Shiloh, Shivaprasad & Simpson 1981), whereas in the present case, as indicated earlier, $\overline{w^2}$ is generally rather higher than $\overline{v^2}$, although the difference is not large. This is illustrated in figure 10, which shows the development of all the

x (cm)	7	17	29	40	47
x/L_r	0.084	0.205	0.349	0.482	0.566
$y(\psi = 0)$ mm	49.5	114.8	147.3	148.6	147.3
$y(\eta = 0)$ mm	59.7	113.0	151.6	157.5	165.6
Λ/L_r	0.063	0.081	0.108	0.139	0.165
$-U_N/U_r$	0.225	0.292	0.265	0.315	0.315
$\Delta U/U_r$	1.365	1.562	1.625	1.700	1.695
U_e/U_r	1.140	1.270	1.360	1.385	1.380
$\overline{q^2}/(2\Delta U^2)$	0.11	0.080	0.051	0.047	0.046
$(\overline{uv}/\overline{q^2})_{max}$	−0.042	0.016	0.089	0.118	0.130
$(\overline{v^2}/\overline{u^2})_{max}$	0.377	0.393	0.485	0.574	0.768

x (cm)	64	71	81	87
x/L_r	0.771	0.855	0.952	1.048
$y(\psi = 0)$ mm	99.1	53.3	0	0
$y(\eta = 0)$ mm	157.5	155.4	165.1	191.8
Λ/L_r	0.192	0.201	0.237	0.267
$-U_N/U_r$	0.22	0.08	0.01	0
$\Delta U/U_r$	1.560	1.400	1.300	1.290
U_e/U_r	1.340	1.320	1.290	
$\overline{q^2}/(2\Delta U^2)$	0.053	0.056	0.074	0.050
$(\overline{uv}/\overline{q^2})_{max}$	0.108	0.148	0.141	0.081
$(\overline{v^2}/\overline{u^2})_{max}$	0.806	0.755	0.780	1.110

TABLE 1. Derived quantities at each axial station. $y(\psi = 0)$ refers to the location of the separated streamline. $y(\eta = 0)$ refers to the location of the shear-layer centreline.

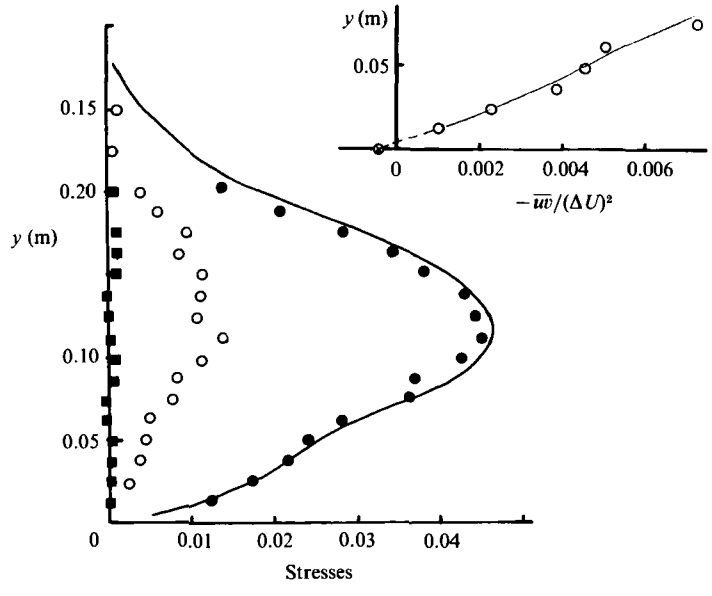

FIGURE 9. Stresses at $x = 47$ cm: ——, $\frac{3}{4}(\overline{u^2}+\overline{v^2})$ $(\Delta U)^2$; ●, $\frac{1}{2}(\overline{u^2}+\overline{v^2}+\overline{w^2})$ $(\Delta U)^2$ (all components measured); ○, $\overline{uv}/(\Delta U)^2$. ■, $\overline{uw}/(\Delta U)^2$. Inset: near-wall region $\overline{uv}$; ⊗, value obtained from wall friction probe.

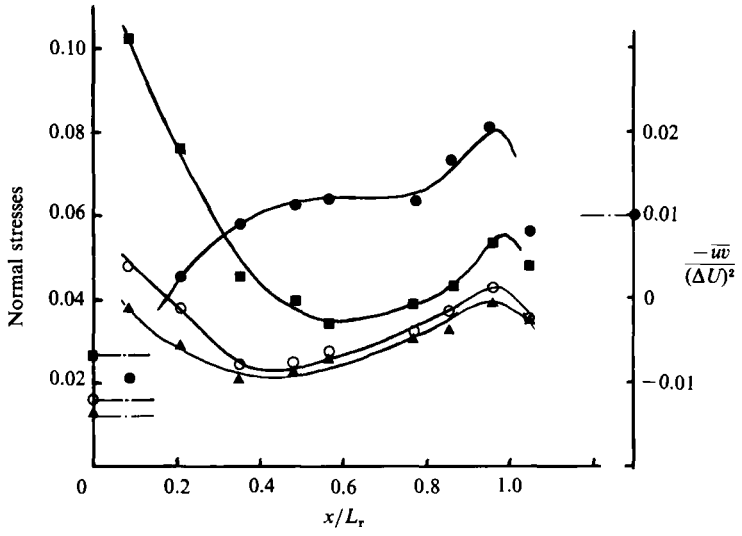

FIGURE 10. Reynolds stresses along line of maximum $\overline{q^2}$. ■, $\overline{u^2}$; ▲, $\overline{v^2}$; ○, $\overline{w^2}$; ●, $\overline{uv}$. All normalized by $(\Delta U)^2$. —·—, Plane-mixing-layer values.

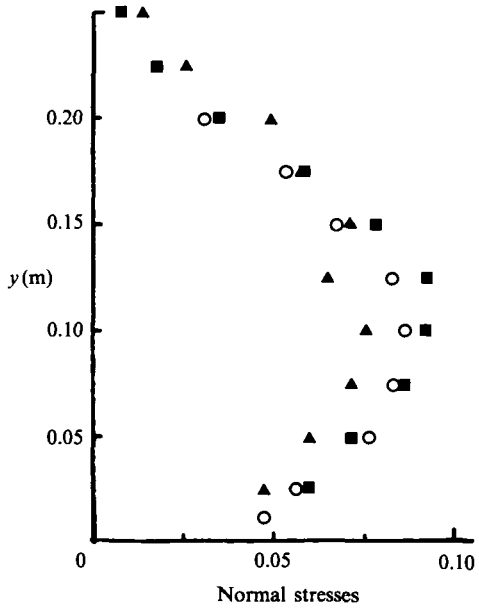

FIGURE 11. Reynolds stresses at $x = 79$ cm ($x/L_r = 0.95$). Legend as in figure 10 but stresses normalized by U_r^2.

Reynolds stresses along the line of maximum $\overline{q^2}$, which can be considered as the approximate centre of the shear layer. (Figure 5 shows that this lies a little on the low-velocity side of the $\eta = 0$ locus – as it does in an ordinary plane mixing layer.) The difference between $\overline{v^2}$ and $\overline{w^2}$ is in fact similar to that found in the separated flow behind a normal flat plate (CH) and it tends to increase in the wall region, particularly as reattachment is approached. This is shown in figure 11, which presents the raw Reynolds normal stresses at a location just prior to reattachment.

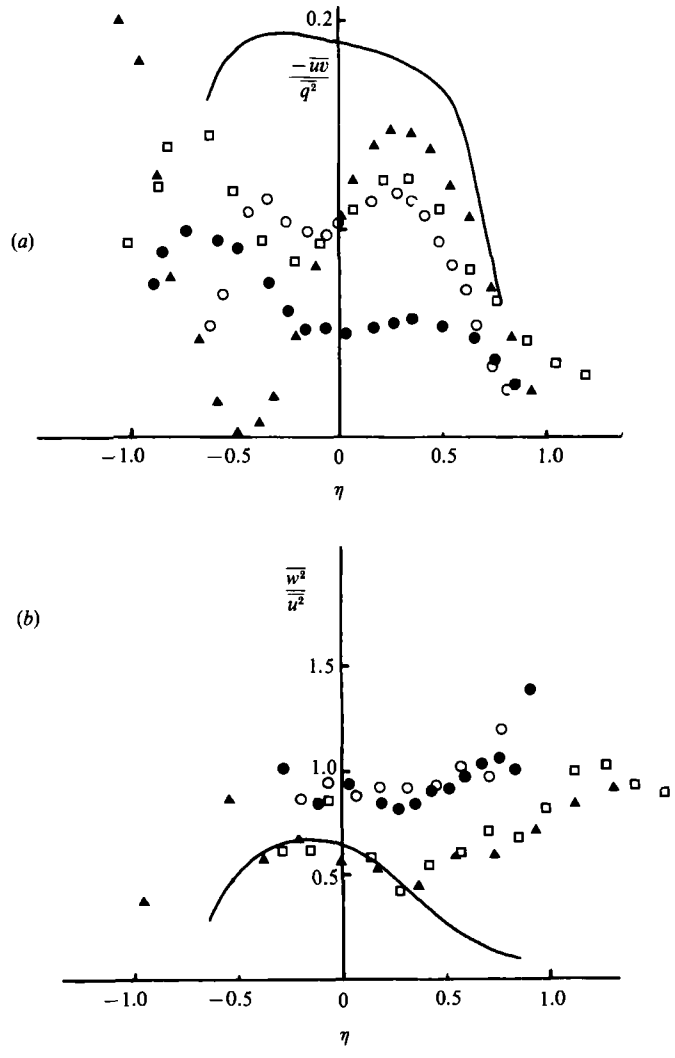

FIGURE 12(a, b). For caption see facing page.

Shiloh *et al.*'s data also show an increase in $\overline{w^2}/\overline{v^2}$ in the near-wall region; indeed one of their three sets of stress profiles obtained in the separated region actually has $\overline{w^2}$ substantially larger than $\overline{v^2}$ over most of the flow.

A significant difference between the present flow and that of CH is the initial abnormally high levels of the Reynolds stresses. In the CH flow, these stresses were not much higher than ordinary plane-mixing-layer values and they all then rose uniformly towards reattachment. In the present case, however, the stresses initially fall rapidly, to reach values at $x/L_r = 0.6$ quite close to those found in CH at the same axial station, before then rising again to reach maxima which, again, occur around reattachment and are quite close to the maxima in the CH flow (see figure 10). The separation process is quite different in the two cases, being, in the present flow, essentially the separation of a fully turbulent boundary layer with a rather curious history. Just upstream of separation, the mean flow curvature is destabilizing and, coupled perhaps with relics of transition, this is probably the major cause of the very

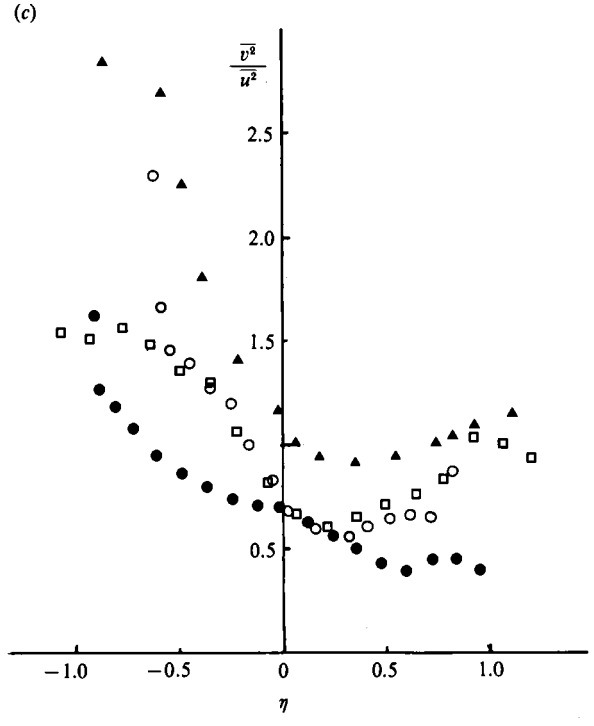

FIGURE 12. Turbulence structure parameters: (*a*) $\overline{uv}/\overline{q^2}$; (*b*) $\overline{w^2}/\overline{u^2}$; (*c*) $\overline{v^2}/\overline{u^2}$. ▲, $x/L_r = 0.20$; □, 0.35; ●, 0.77; ○, 0.87; ——, plane mixing layer.

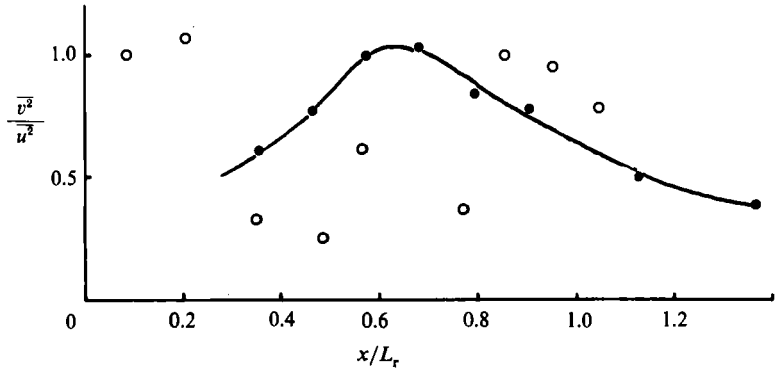

FIGURE 13. Variation of $\overline{v^2}/\overline{u^2}$ along a line parallel and close to the wall ($y/L_r = 0.01$): ●, CH; ○, present flow.

high Reynolds stresses in the flow at separation. Around separation itself the curvature ($1/R$) changes sign and becomes relatively large so the subsequent fall in all the Reynolds stresses may simply be a result of the stabilizing curvature. In Simpson's flow, the streamline curvature was destabilizing over nearly all the measured region – which did not extend to anywhere near reattachment – and the Reynolds stresses all rise up to the last measuring station. Upstream of separation, this must be due at least partly to curvature effects, but further downstream curvature may be much less significant than the effects of re-entrainment of stress-bearing fluid, as was the case in the CH flow (see below).

Near the wall one expects $\overline{v^2} < \overline{u^2}$, if only because of the impermeability condition at $y = 0$. It has been shown previously that in the case of the normal flat-plate flow, whilst this *is* certainly true throughout the separated region (near the wall), the structure parameter, $\overline{v^2}/\overline{u^2}$, actually rises in the wall region as reattachment is approached (CH). In figure 12 the turbulence structure parameters, $\overline{uv}/\overline{q^2}$, $\overline{w^2}/\overline{u^2}$ and $\overline{v^2}/\overline{u^2}$, are plotted as a function of cross-stream coordinate, η, and figure 12(*c*) shows that this feature of an initially rising $\overline{v^2}/\overline{u^2}$ does not occur in the present case. It was argued in CH that $\overline{v^2}$ is the first normal stress to respond to wall influence and actually first rises as the shear layer approaches the wall, as Wood & Bradshaw (1982) have shown that it does for a shear layer approaching a wall on the *high*-velocity side. Re-entrainment of stress-bearing fluid returned upstream around reattachment enhances the energy levels further and this 'positive feedback' mechanism is eventually limited because $\overline{v^2}$ clearly cannot go on rising; *very* near the wall, of course, it must always fall. Now in the present case, the shear layer is relatively very much closer to the wall throughout the entire extent of the separation zone, so the more obvious damping effect of the wall dominates. The variation of $\overline{v^2}/\overline{u^2}$ along a line close and parallel to the wall, shown in figure 13, reinforces this argument. It is clear that whilst in the CH flow this ratio first rises before falling in the reattachment zone, in the present case it has the opposite behaviour.

On the other hand, the behaviour of $\overline{w^2}/\overline{u^2}$ is very similar to that found by CH throughout the flow. In particular, the preferential amplification of $\overline{w^2}$ as reattachment is approached is very clear (figure 12*b*); the fact that the shear layer is closer to the wall does not alter, for $\overline{w^2}$, the qualitative operation of the feedback mechanism referred to above. Further, the trend in $\overline{v^2}/\overline{u^2}$ in the central region (around $\eta = 0$) and on the high-velocity side ($\eta < 0$) is also similar to that in the normal flat-plate flow. $\overline{v^2}/\overline{u^2}$ tends to fall with increasing x, although in the early part of the flow the levels in the outer part of the flow start much higher than those typical of a plane mixing layer. This is probably a result of the initial destabilizing curvature around separation.

The behaviour of $\overline{uv}/\overline{q^2}$ (figure 12*a*) is largely similar to that found by CH, except that near separation it is substantially lower than ordinary plane-mixing-layer or boundary-layer values across the whole flow, whereas in the CH flow it was initially similar to these levels in the outer region. This is probably another result of the unusual history of the boundary layer in the present case – the strongly destabilizing curvature leading to relatively large increases in $\overline{q^2}$ compared with $\overline{uv}$. Our present $\overline{uv}/\overline{q^2}$ data are also similar to the data of Shiloh *et al.* (1981), including the presence of a significant 'dip' in $\overline{uv}/\overline{q^2}$ in the centre of the flow around $x/L_r = 0.5$.

Overall we conclude that the flow in the downstream half of the separation region ($0.5 < x/L_r < 1.0$), at least as far as the behaviour of the Reynolds stresses is concerned, is similar to that in the same region of the normal flat-plate flow, despite the very different initial conditions. The exception – the response of the normal stress component ($\overline{v^2}$) – can be explained on the basis that the wall influence extends much further upstream in the present case. Stress behaviour further upstream ($x/L_r < 0.5$) will depend on how far the effects of the re-entrainment of upstream-propagating fluid returned around reattachment can dominate over other more local effects, like flow curvature. This will in turn depend, to some extent at least, on the nature of the separation process. We return to these points in due course.

Turning now to the higher-order moments, figure 14 shows the development of the minimum and maximum values of the quantities $(\overline{v^3} + \overline{u^2 v})$ and $(\overline{u^3} + \overline{uv^2})$, normalized by $(\Delta U)^3$. The major points to note are the initial very high levels of the latter,

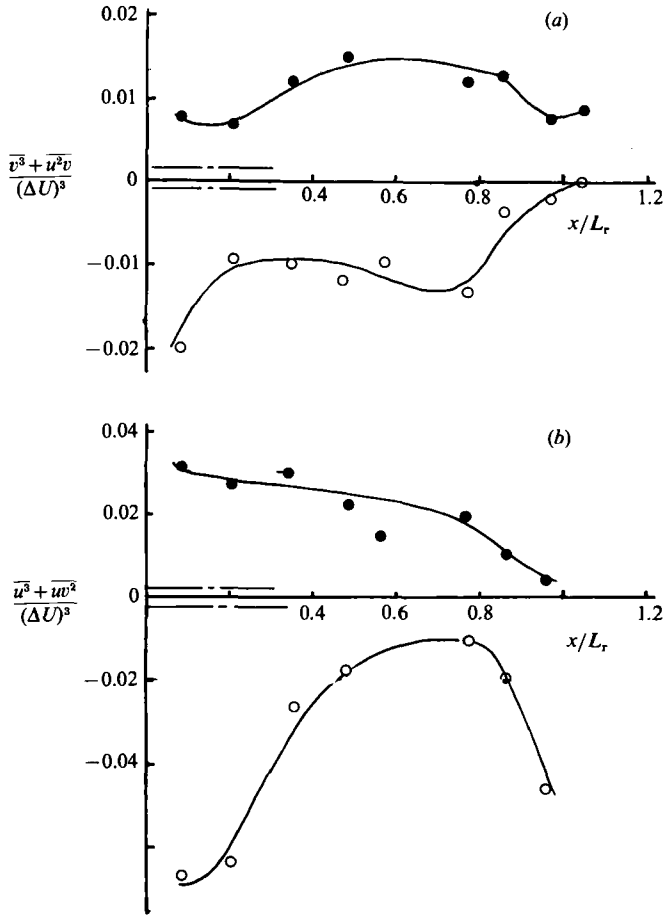

FIGURE 14. Maximum (●) and minimum (○) values of velocity triple-products sums. (*a*) $(\overline{v^3}+\overline{u^2v})/(\Delta U)^3$; (*b*) $(\overline{u^3}+\overline{uv^2})/(\Delta U)^3$. — · —, Plane-mixing-layer values.

particularly in the early part of the flow, and the fact that throughout the flow both quantities are generally much larger than the equivalent quantities in the ordinary plane mixing layer. In a boundary layer, of course, all the triple products are more than an order of magnitude smaller than in a plane mixing layer and take positive values only – for y increasing away from the wall. Only beyond reattachment do we expect all the triple products to have one sign (negative here because $\eta \propto -y$) and the data are consistent with that behaviour.

Abnormally large triple products imply large turbulent transport; if the pressure transport for turbulent energy is small, the transport velocity is $V_q = \overline{q^2v}/\overline{q^2}$ and a reasonable approximation to this is provided by the measured value of $V'_q = (\overline{v^3}+\overline{u^2v})/(\overline{u^2}+\overline{v^2})^{\frac{3}{2}}$. Cross-stream profiles of V'_q, normalized by ΔU, are shown for various axial stations in figure 15. It is clear that on the low-velocity (wall) side of the flow values do not generally exceed the plane-mixing-layer maximum, whereas on the high-velocity side very large transport velocities occur around the central region of the recirculation zone. The implication would seem to be that the large-eddy processes, which in an ordinary mixing layer are those which contribute most to transport of energy away from the centre of the flow, may be considerably

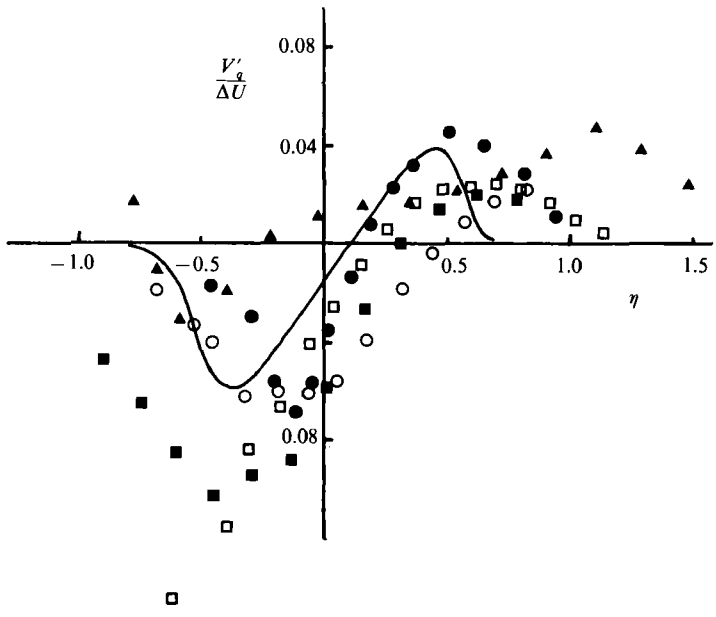

FIGURE 15. Profiles of turbulence energy transport velocity. ▲, $x = 17$ cm, $x/L_r = 0.2$; □, 40 cm, 0.48; ●, 64 cm, 0.77; ■, 71 cm, 0.86; ○, 79 cm, 0.95; ——, plane-mixing-layer values.

enhanced in the present flow. This conclusion is perhaps consistent with the view that around reattachment large eddies are intermittently returned upstream and (after being heavily distorted) are re-entrained into the shear layer. On the other hand, a typical measure of large-eddy strength,

$$\{(\overline{v^3}+\overline{u^2v})_{\max}-(\overline{v^3}+\overline{u^2v})_{\min}\}/(\overline{u^2}+\overline{v^2})^{\frac{3}{2}},$$

is quite similar in the present flow to its value in the plane mixing layer, although it must be recognized that the measurement of this quantity is rather less precise in the present case than it is in thin shear layers. It is worth noting here that the triple-product profiles (e.g. figures 2 and 8*b*) are very similar in form to those of Driver & Seegmiller (1985) obtained by laser-Doppler anemometry in the recirculating region behind a backward-facing step.

Note, finally, that all the stresses and triple products have been presented in the usual laboratory coordinates, despite the fact that the local mean flow direction is not generally parallel to the x-axis. As pointed out by CH, discussion of individual stresses is, in fact, only meaningful at all if a general shear-layer direction is apparent. Whilst different definitions of shear-layer direction do not coincide closely over the whole flow, there *is* a clear qualitative direction of flow development. It was found in the present case that rotating the individual stresses to align them with local shear-layer axes (defined, for example, by the direction of the line of maximum $\overline{q^2}$) made no qualitative difference to the behaviour demonstrated in the figures discussed above. This was also true in the CH flow, and justifies the relevance of the arguments outlined earlier.

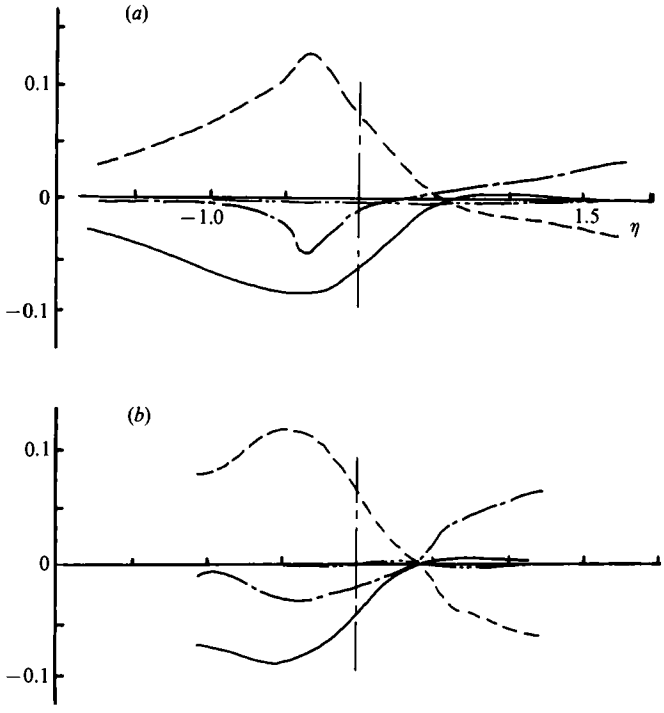

FIGURE 16. y-direction momentum balances at (*a*) $x = 29$ cm, $x/L_r = 0.35$; (*b*) 47 cm, 0.57. ——, $(U\partial V/\partial x + V\partial V/\partial y)$; — · —, $\partial\overline{v^2}/\partial y$; — · · —, $\partial(\overline{uv})/\partial x$; – – –, $\partial p/\partial y$. All terms are normalized using ΔU and Λ.

5. Momentum and turbulence energy balances

The x- and y-direction momentum equations are, respectively,

$$U\left(\frac{\partial U}{\partial x}\right)+V\left(\frac{\partial U}{\partial y}\right) = -\frac{1}{\rho}\frac{\partial p}{\partial x}+\frac{\partial(-\overline{uv})}{\partial y}-\frac{\partial\overline{u^2}}{\partial x}, \tag{2}$$

$$U\left(\frac{\partial V}{\partial x}\right)+V\left(\frac{\partial V}{\partial y}\right) = -\frac{1}{\rho}\frac{\partial p}{\partial y}+\frac{\partial(-\overline{uv})}{\partial x}-\frac{\partial\overline{v^2}}{\partial y}. \tag{3}$$

The viscous terms have been omitted since these are small nearly everywhere. With the exception of the pressure gradients, all the terms can be deduced from the measurements. The resulting momentum balances are qualitatively similar to those presented by CH and the following features are particularly noteworthy.

For Simpson's flow, in the region (near the wall) where $\partial(-\overline{uv})/\partial y$ is positive, (3) reduced to

$$-\frac{1}{\rho}\frac{\partial P}{\partial y} = \frac{\partial\overline{v^2}}{\partial y}, \tag{4}$$

both upstream and downstream of separation. Figure 16, in which (typical) y-direction momentum balances at $x/L_r = 0.35$ and 0.57 are presented, shows that the same is true in the present case. Only in the central and outer region of the flow is the convective term significant and, as in Simpson's case, here it is significantly larger than the normal stress gradient. Note also that the axial shear stress gradient is everywhere negligible.

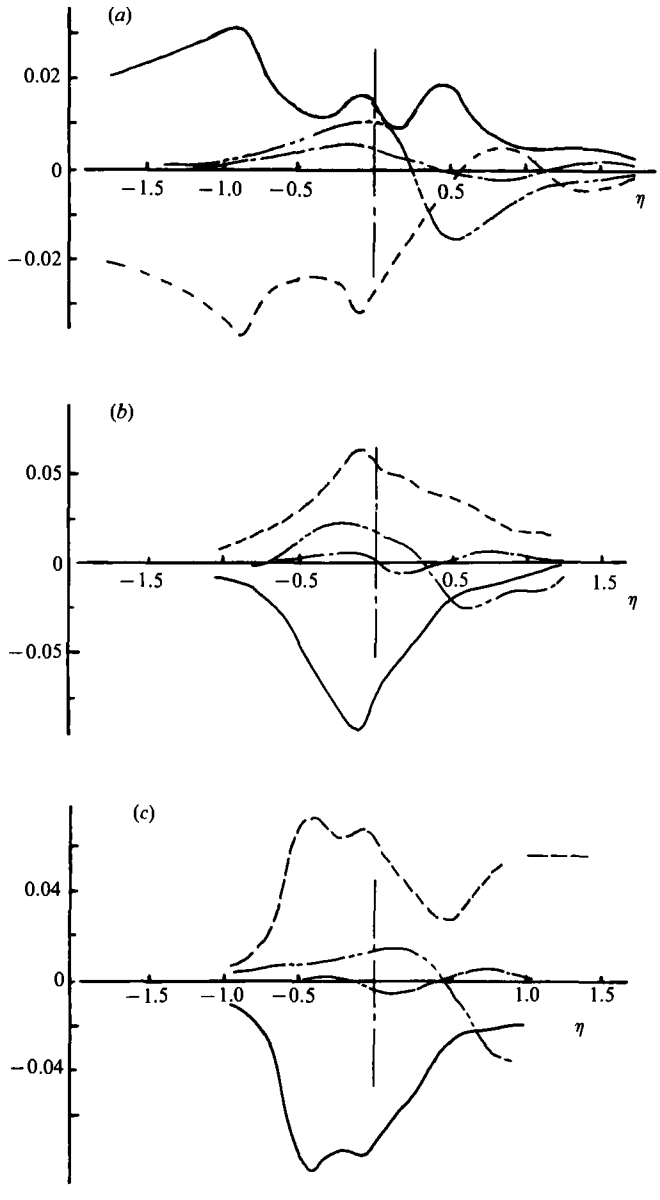

FIGURE 17. x-direction momentum balances at (*a*) $x = 29$ cm, $x/L_r = 0.35$; (*b*) 47 cm, 0.57; (*c*) 64 cm, 0.77. ——, $(U\partial U/\partial x + V\partial U/\partial y)$; — - - —, $\partial \overline{u^2}/\partial x$; — · · · —, $\partial(\overline{uv})/\partial y$; - - - -, $\partial p/\partial x$. Surface pressure gradient is small and not shown in (*a*) and (*b*), but significant in (*c*). Normalization as in figure 16.

Integration of (4) shows that $P(x, y) = P_0 - \rho\overline{v^2}$, where P_0 is the wall mean static pressure. If $\partial\overline{v^2}/\partial x$ is much smaller than $\partial P_0/\partial x$, the mean pressure gradient will therefore be nearly independent of y in this region where $\partial(-\overline{uv})/\partial y$ is positive. This was true over most of the flow studied by Simpson but is not so in the present case, as demonstrated by the x-direction momentum balances at $x/L_r = 0.35$, 0.57, 0.77, shown in figure 17. The wall static pressure is roughly constant over the central part of the recirculating region and $\partial\overline{v^2}/\partial x$ is relatively significant. As pointed out

previously, Simpson did not make measurements beyond about $x/L_r = 0.5$; $\partial P_0/\partial x$ was therefore positive throughout the most downstream part of the flow that he investigated.

$\partial P/\partial x$ in figure 17 was obtained by difference and it is encouraging that near the wall the value asymptotes to the $\partial P_0/\partial x$ deduced from the measurements of the wall mean static pressure (see figure 17*c* for an example). Note that measurements of the other terms are not available within the very thin boundary-layer region; $\partial(-\overline{uv})/\partial y$ may not balance $(1/\rho)\,\partial p/\partial x$ exactly at the wall because there the viscous term (omitted from (2) and (3)) may be significant. The various 'humps and bumps' in the convective term, particularly noticeable at $x/L_r = 0.35$ and 0.77, are caused by the relatively large contribution made by $V\partial U/\partial y$, arising from the fact that at these locations there is a significant mean V-component (unlike the ordinary plane-mixing-layer case). Note that the total convective terms are of opposite sign at these locations – because V is of opposite sign – and that the contributions from the stress terms are not large enough to prevent the pressure-gradient term largely following these humps.

The turbulence energy equation is

$$U\frac{\partial(\frac{1}{2}\overline{q^2})}{\partial x}+V\frac{\partial(\frac{1}{2}\overline{q^2})}{\partial y}=-\overline{uv}\left[\frac{\partial U}{\partial y}+\frac{\partial V}{\partial x}\right]-(\overline{u^2}-\overline{v^2})\frac{\partial U}{\partial x}-\frac{\partial}{\partial x}\left[\overline{\tfrac{1}{2}q^2u}+\frac{\overline{p'u}}{\rho}\right]-\frac{\partial}{\partial x}\left[\overline{\tfrac{1}{2}q^2v}+\frac{\overline{p'v}}{\rho}\right]-\epsilon,$$

where the symbols have their usual meaning and the viscous terms have been neglected, as usual. Qualitatively this equation can be expressed as

Advection (by Mean Flow) = – Production (by shear and normal Reynolds stresses) – Transport (by Turbulence) – Dissipation.

In an ordinary plane mixing layer, the energy balance is characterized by: (i) a balance in the central region of the flow between energy production (a gain) and turbulence transport and dissipation (a loss); the latter two are of the same order; (ii) a balance in the outer regions – both on the low- and the high-velocity sides – between advection (a loss) and turbulent transport (a gain); (iii) production by the normal stresses which is small compared to that by the shear stress across the entire flow; (iv) pressure transport which is usually reckoned to be insignificant, since measured dissipation leads to approximate balance with all other terms (figure 18*d*).

In the present case all terms except the dissipation and the pressure transport could be estimated from the measured data, using, in the case of the turbulent transport terms, the approximations for the velocity triple-product terms discussed earlier. Estimates of gradients, particularly $\partial(\frac{1}{2}\overline{q^2u})/\partial x$, are inevitably somewhat uncertain, but we believe that the qualitative behaviour of the cross-stream balances shown in figure 18 is correct. The dissipation term has in each case been deduced by difference from the other terms, which implies the assumption that pressure transport is insignificant. This is discussed in due course. There are a number of noteworthy features of the balances.

First, in all three cases presented ($x/L_r = 0.2$, 0.57 and 0.86), gain by turbulent transport is the largest of the measured terms in the near-wall region ($\eta > 0.4$–0.6). This is similar to the result of Driver & Seegmiller (1985) for the flow behind a backward-facing step and confirms the conclusion of Simpson *et al.*, who found that the shear and normal stress production and also the advection terms were relatively small in the backflow region, so that turbulence energy reaches this region largely via

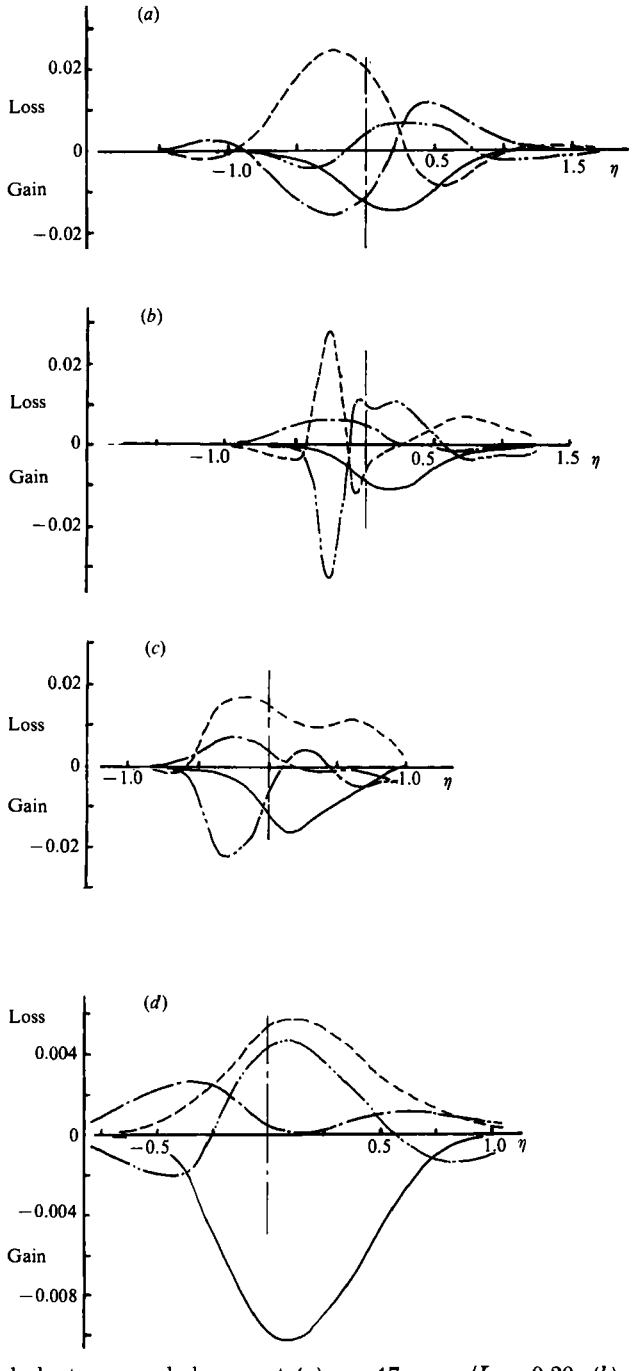

FIGURE 18. Turbulent energy balances at (*a*) $x = 17$ cm, $x/L_r = 0.20$; (*b*) 47 cm, 0.57; (*c*) 71 cm, 0.86. (*d*) Plane mixing layer. —·—, Advection; ——, production; —··—, diffusion; – – –, dissipation (by difference). All terms are normalized using ΔU and Λ.

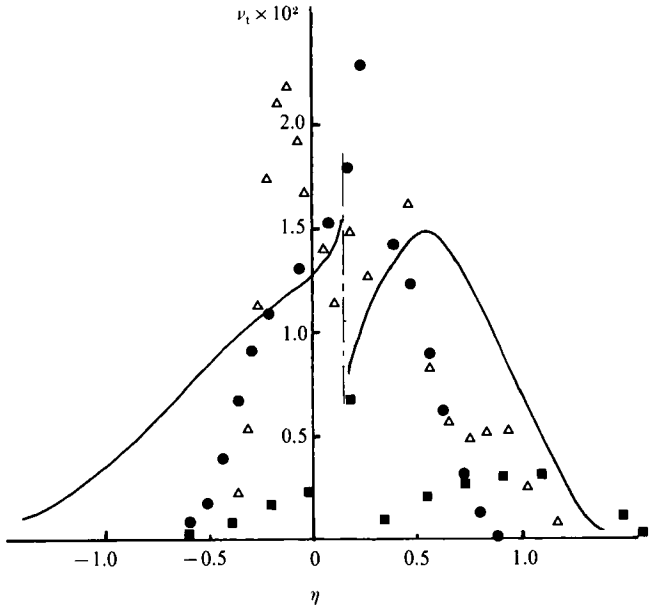

FIGURE 19. Profiles of eddy diffusivity. ■, $x = 17$ cm, $x/L_r = 0.20$; △, 47 cm, 0.57; ●, 71 cm, 0.86; ——, plane mixing layer. (All normalized using ΔU and Λ.)

turbulent diffusion, although they were not able to measure this diffusion directly. Actually, the shape of the (total) transport cross-stream profile is qualitatively similar at all stations to that in a plane mixing layer. The energy balance in this latter case is shown for reference in figure 18(*d*) using for convenience data from Castro (1973), which Rodi (1975) states are representative. Throughout the flow, energy is transported from the central region (around $\eta = 0$) to the low- and high-velocity edges of the shear layer. It is noticeable that in the outer (high-velocity) region the gain of turbulence energy by diffusion rises to a maximum around the central part of the recirculation region – $x/L_r \approx 0.5$, compare figures 18(*a*), 18(*b*) and 18(*c*) – whereas the loss around $\eta = 0$ is a maximum near reattachment. Unlike a thin shear flow, the contribution from $\partial(\frac{1}{2}\overline{q^2 u})/\partial x$ to the total diffusion transport is not negligible, so that the cross-stream integral of the total transport does not sum to zero as it does for a plane mixing layer.

Although, in common with other workers, we have used the term 'turbulent diffusion', it must be recognized that nowhere in this flow is the turbulent transport like a gradient diffusion process. Even in thin shear flows, some authors (notably Bradshaw – see Bradshaw 1967, for example – following Townsend, 1956) prefer to consider the turbulent transport in terms of a transport velocity generated essentially by the large-eddy motions. In separated flows, there is no doubt that such a concept is likely to be even more appropriate than in thin shear flows. Figure 19, which shows profiles of the eddy diffusivity, $\overline{q^2 v}/(\partial \overline{q^2}/\partial y)$, emphasizes the lack of 'diffusion-like' behaviour.

The large energy gain via the transport processes on the high-velocity side in the central part of the recirculation region, noted above, is consistent with the very large transport velocities in that region (figure 15). It seems likely that these are caused by particularly energetic large-eddy motions, despite the presence of significant stabilizing curvature in the first half of the flow. This further emphasizes the

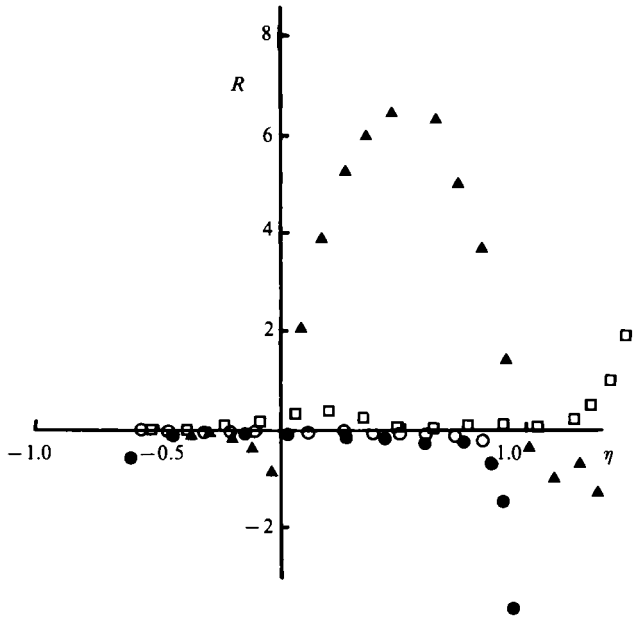

FIGURE 20. Ratio (R) of normal to shear stress production terms ($R = [(\overline{u^2}-\overline{v^2})\partial U/\partial x]/[-\overline{uv}(\partial U/\partial y+\partial V/\partial x)]$. ▲, $x = 17$ cm, $x/L_r = 0.2$; □, 29 cm, 0.35; ●, 64 cm, 0.77; ○, 71 cm, 0.86.

dominant effect of the whole reattachment region, where high-energy fluid is returned and fed back into the shear layer.

The second point to note about the energy balances is the behaviour of the production term. As far as the total production is concerned, this is qualitatively very similar throughout the flow to the plane-mixing-layer behaviour, in that maximum production occurs in the central region of the layer. However, unlike thin shear flows, there are regions where production by the normal stresses is very significant. Figure 20 shows the ratio of normal stress to shear stress production, $[(\overline{u^2}-\overline{v^2})\,\partial U/\partial x]/[-\overline{uv}\,\partial U/\partial y]$, at various axial stations. Simpson, Strickland & Barr (1977) call this ratio $(F-1)$. Whilst it is significantly less than unity over much of the flow, both near the wall and across the whole layer in the first part of the recirculating zone, energy production via normal stresses considerably exceeds that by the shear stress. Near the wall, this is largely because $\partial U/\partial y$ becomes small (and changes sign, although shear stress measurements could not be made that close to the wall). The results are similar to Simpson's in that respect. At $x/L_r = 0.2$, however, the very large values of $(1-F)$ occur because $\partial U/\partial x$ is relatively large (and negative) and, simultaneously, $\overline{u^2}$ is much larger than $\overline{v^2}$. This is unlike Simpson's data, since in his case the separation was much less rapid and mean flow curvature was relatively mild. In contrast, at the other end of the recirculating region, although $\partial U/\partial x$ has a similar (but positive) magnitude, $\overline{u^2}$ and $\overline{v^2}$ are not very different (see figure 12b), so that the normal stress production is similar to its value further upstream. Note that rotating the velocity components to be consistent with the direction of the local shear layer, although it reduces these significant variations in $(F-1)$, does not alter the conclusion that normal stress production is large in certain regions of the flow.

The final point to make concerns the behaviour of the dissipation, deduced as the difference in the measured terms. Figures 18(a) and 18(b) show that the resulting estimates of the dissipation profiles have negative lobes on both sides of the central

region of the shear layer. Since (i) the actual dissipation must always be positive and (ii) errors in the measured triple velocity transport are certainly lower than 100%, we have to conclude that the pressure–velocity correlation component of the energy transport must be significant. Indeed, it must in those regions be of the same order as the velocity triple-product transport components, to ensure $\epsilon > 0$. It therefore seems very likely that pressure transport is important across the whole flow, at least at these stations, and there appears to be no guarantee that this is not the case nearer reattachment, although here the deduced dissipation remains positive (figure 18*c*). The 'dip' in the apparent dissipation at $x/L_r = 0.86$ may well be caused more by changes in the size of the pressure transport term, rather than any true multi-peaked behaviour of the actual energy dissipation. It is interesting that the energy balance obtained by Driver & Seegmiller (1985) in the recirculating region behind a backward-facing step also has a distinct dip in the dissipation profile, although it does not become negative, so the (neglected) pressure–velocity transport may be relatively smaller in that flow.

6. Timescales

As indicated earlier, one of the features of nearly all the published work on nominally two-dimensional separated regions is the finding that a distinct low-frequency motion exists, whose characteristic timescale is very much longer than that associated with the large eddies in the separated shear layer. This motion is usually most clearly identified just downstream of separation, where the corresponding spectral peak is well separated from the shear-layer turbulence, and has been noted by Castro (1981), Eaton & Johnston (1982), Kiya & Sasaki (1983), Cherry *et al.* (1984), Barkey-Wolf (1987) and CH, among others. To find whether a similar motion occurred in the present case, autocorrelation measurements were made at $x/L_r = 0.2$, using the techniques described by Castro (1985). Typical results are presented in figure 21 and the resulting cross-stream variation in integral timescale, defined by

$$T_x = \int_{\infty}^{\tau'} R(\tau)\, \mathrm{d}\tau,$$

is shown in figure 22. τ' is the time to the first zero crossing of $R(\tau)$, or ∞ if there is no zero crossing and T_x has been normalized by ΔU and A. The maximum value of T_x occurs in the centre of the shear layer and is somewhat larger than the maximum value of about 10 implied by the data of CH and Kiya & Sasaki (1983) at an equivalent distance from separation ($x/L_r = 0.2$). The immediate implication is that a similar low-frequency motion is present. This is corroborated by the wall pressure spectrum obtained at the separation position, shown in figure 23. Because of acoustic interference, this kind of data was not easy to obtain; in fact, similar measurements a little further downstream were rather more uncertain (largely because the total mean-square fluctuating pressure was much smaller there), so are not presented, although the low-frequency peak evident in figure 23 was just as clear.

In terms of the equivalent autocorrelation timescale (see CH for a discussion of such equivalence) this low-frequency peak corresponds to a $T_x \Delta U/A$ value which lies remarkably close to that obtained by extrapolating to the wall the timescales obtained from the velocity autocorrelations, as shown in figure 22. This is rather smaller than the timescale deduced by Kiya & Sasaki (1983), also from a pressure spectrum, and it appears that although the maximum value in the centre of the layer

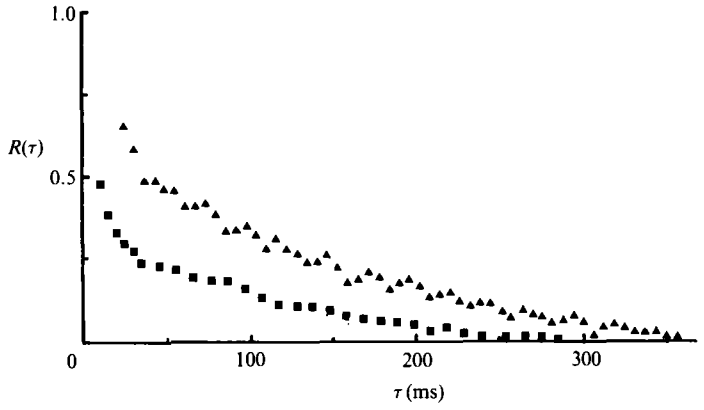

FIGURE 21. Examples of velocity autocorrelation measurements at $x = 17$ cm, $x/L_r = 0.20$. ■, $y = 126$ mm; ▲, 51 mm.

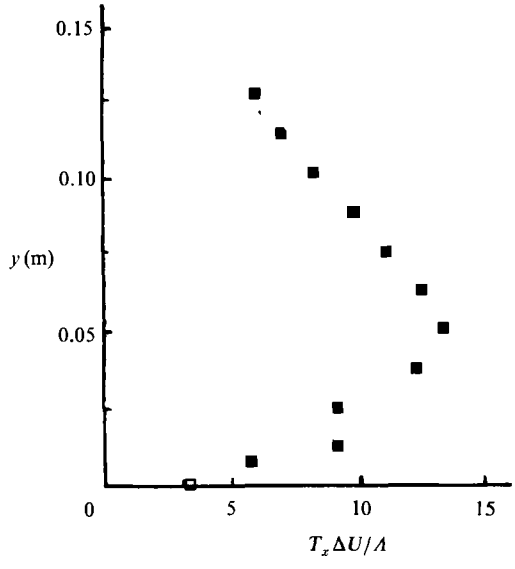

FIGURE 22. Variation of the longitudinal integral timescale across the flow: ■, from velocity autocorrelations; □, from wall pressure spectrum.

is similar to that found previously, the variation across the flow is rather lower. This suggests that the 'flapping' motion which produces the low-frequency peak is rather more energetic in the present flow – partly perhaps because the separation point is not fixed; unsteadiness in the separation location would lead to 'apparent' flapping of the shear layer. It would also, of course, be a contributory cause of the higher values of the Reynolds stresses in the region just after separation. The fact that the timescale deduced from the fluctuating wall pressure signal is close to those found from velocity measurements suggests that both are dominated by large-eddy motions, for the former must contain contributions from far-field fluctuations whereas the latter do not.

Note also that the higher frequency peak in the pressure spectrum has a timescale an order of magnitude larger than the low-frequency peak and *is* representative of the more usual large-eddy motions in the shear layer. It is more noticeable than it

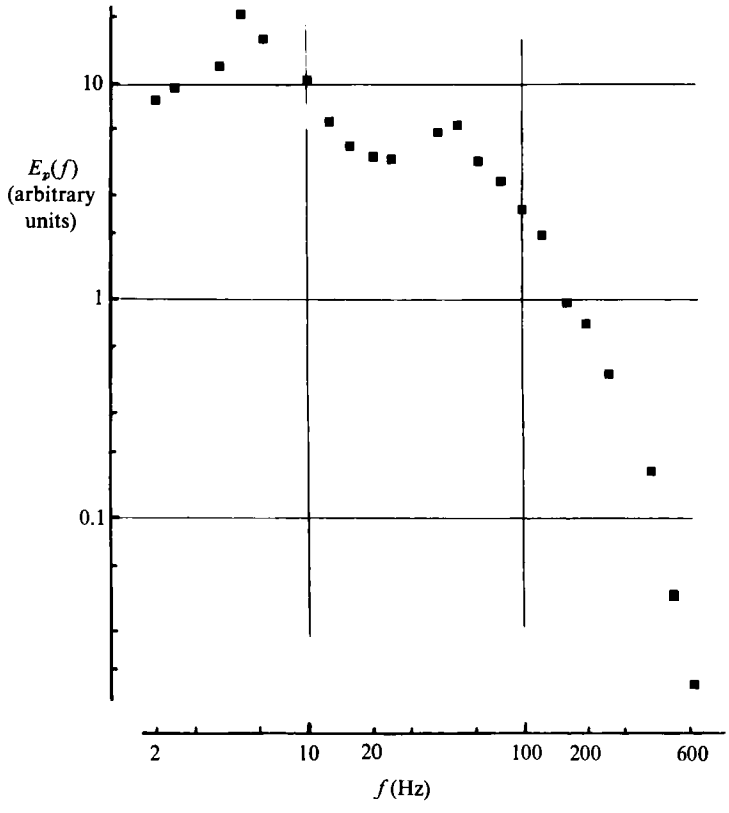

FIGURE 23. Fluctuating wall pressure spectrum at $x = 0$ (separation).

would have been in the CH flow, because the shear layer is relatively much closer to the surface in the present case. In that respect, the present flow is more like that studied by Kiya & Sasaki (1983) and Cherry *et al.* (1984), who also found two widely separated and very clear peaks in the wall pressure spectrum just downstream of separation.

Although time did not permit further autocorrelation or pressure spectral measurements further downstream, there seems sufficient evidence to conclude that this flow is similar to other separated flows in respect of the presence of a very noticeable low-frequency motion. Although there is some controversy over the precise cause of this motion, it seems generally agreed that it must be driven by an interaction between the processes around reattachment and the upstream shear layer (Kiya 1988). In the present case, as noted above, it may be further enhanced by unsteadiness in the separation process.

7. Final comments, implications and conclusions

The results presented and discussed in the previous sections demonstrate that this separated flow has some features similar to, and others dissimilar to, separated flows generated under different conditions. Compared with the separated boundary layer extensively studied by Simpson and his colleagues, the present flow is produced by a much more adverse pressure gradient. Although it consequently has some characteristics which are very different, there are certain similarities. These include:

(i) the importance of the normal stresses in turbulence energy production near the wall;

(ii) the relatively large influence of turbulent transport, which cannot be adequately described in terms of the usual gradient diffusion process.

Other features either show significant differences or cannot be compared directly with Simpson's flow since he did not make measurements downstream of about the first third of the recirculating region, nor did he obtain velocity triple-product data within the backflow region. These include:

(i) the initially very much higher Reynolds stresses just beyond separation;

(ii) the rise (after an initial rapid fall) in Reynolds stresses as reattachment is approached, where the three normal stresses become more nearly equal;

(iii) the significant contribution of the axial gradient of $\overline{q^2u}$ to the turbulence energy transport in the backflow region;

(iv) the apparently large contribution of the pressure–velocity correlation to the turbulent transport – modelling procedures would presumably need to take that into account in some way;

(v) the fact that the ratio of the thickness of the backflow region to the total shear layer thickness is much larger in the present flow – leading to a much higher probability that the mean backflow at stations not far from separation comes from far downstream (as also found by Fox & Kline 1962, in wide angle diffuser flows).

Furthermore, many features of the present flow are similar to those found in other separated flows generated by a quite different process – notably the 'normal flat plate plus splitter plate' flow of Ruderich & Fernholz (1986) and CH, the 'blunt plate' flows of Kiya & Sasaki (1983), Cherry *et al.* (1984) and Barkey-Wolf (1987), and backward-facing-step flows studied by, for example, Eaton & Johnston (1982) and Adams & Johnston (1988). These features include the following.

(i) The fact that the turbulence structure of the separated shear layer, whilst certainly closer to that of a plane mixing layer than that of a wall boundary layer, has characteristics quite different from either. Structure parameters like $\overline{uv}/\overline{q^2}$ and $\overline{v^2}/\overline{u^2}$ respond markedly to the re-entrainment of turbulent fluid transported upstream from the reattachment region. There is evidence that this response is largely independent of the separation process, so that the structure of the reattachment region may be fairly universal.

(ii) There is significant low-frequency motion present in the flow. Of the authors listed above, only Ruderich & Fernholz did not notice such a motion, although they did not specifically look for it. More recently Jaroch & Fernholz (1989), studying the same flow as CH and Ruderich & Fernholz, also report not finding any very-low-frequency motion. The reasons for this difference are unclear.

(iii) Note also that, although not discussed in this paper, Dianat & Castro (1989) demonstrated the absence of any logarithmic region in the thin wall layer beneath the recirculation zone. Velocity profiles here do not scale on viscous wall units, but collapse quite well using Devenport's (1985) correlation. The wall skin friction, normalized using the local maximum negative (backflow) velocity, is inversely proportional to the square root of the Reynolds number based on the same velocity and the distance from reattachment. Different geometries yield identical behaviour, although not identical skin friction values (see Dianat & Castro 1989; Castro *et al.* 1988 and Adams & Johnston 1988, for further discussion).

In view of the unusual history of the present boundary layer just prior to separation, the impossibility of obtaining detailed data in that region, and the

possible influence of three-dimensionality as reattachment is approached, the present flow is not a particularly suitable one for detailed comparison with numerical predictions. However, there are a number of features of the results which, as detailed above, emphasize the conclusions reached in previous studies and, in particular, suggest that nominally two-dimensional flows, however produced, have important features in common. These features have definite implications for turbulence models.

For example, it seems beyond dispute that, in the context of 'universal' models, complete Reynolds stress modelling will be required for accurate prediction of such flows. The very different behaviour of the individual stresses as reattachment is approached, and the consequent effects on the upstream shear layer via the re-entrainment process, could not possibly be adequately represented by models which implicitly assume stress isotropy and solve a transport equation for total turbulence energy. Whilst, from an engineering point of view, this may not be too important if only overall quantities, like the distance to reattachment, are required, it will certainly be critical if accurate prediction of, say, skin friction beyond reattachment, or surface heat transfer anywhere, is needed.

Further, gradient diffusion models are unlikely to be able to represent the large-eddy turbulent transport processes that are so dominant in some regions of the flow. Indeed, since it appears that the fluctuating pressure–velocity correlations contribute strongly in some regions, the more obvious replacement of gradient diffusion by simple transport velocity ideas will also presumably be inadequate. In a recent study of turbulence models for separated flows Amano, Goel & Chai (1988) have shown that a fairly standard Reynolds stress closure significantly underpredicts the turbulent transport and they therefore proposed using a model in which the triple products are calculated directly from their own transport equations. This approach avoids gradient diffusion models for $u_i u_j u_k$, at the expense of considerable added complexity, and seemed to predict triple products in reasonable agreement with the measurements of Driver & Seegmiller (1985). However, it involved other, arguably questionable assumptions and took no specifically different account of the contribution from the pressure–velocity transport term.

Flows like these are essentially overwhelming perturbations (in the sense of Bradshaw & Wong 1976), in which a thin shear flow changes type – from a boundary layer to a mixing layer. But the mixing layer has characteristics quite distinct from those of an ordinary plane mixing layer; it cannot even be considered as a 'simple' distortion of the latter since we have shown that generally the reattachment processes affect the flow upstream more strongly than, say, mean flow curvature (and in the opposite direction). In that this reattachment region may have a fairly universal structure, there is some hope, perhaps, that a zonal approach could be developed, in which the reattachment zone is one of the basic building blocks (zones) from which the whole flow is constructed.

On the other hand, the presence of very-low-frequency motions arguably suggests that any turbulence model based on time-averaged equations may be inappropriate for such flows. It remains to be seen whether such motions are unique to (nominally) two-dimensional flows but, in any case, the dominance of large-eddy structures is likely to be universal and any effective modelling procedure cannot afford to ignore their influence.

The financial support of the Procurement Executive, Ministry of Defence is gratefully acknowledged. We are also indebted to the technical staff of the Department of Mechanical Engineering, to our colleague Dr P. E. Hancock for

valuable discussions, and to Mr T. Laws, without whose particular technical skills much of the work would have been impossible.

REFERENCES

ADAMS, E. W. & JOHNSTON, J. P. 1988 Flow structure in the near-wall zone of a turbulent separated flow. *AIAA J.* **26**, 932–939.

ADAMS, E. W., JOHNSTON, J. P. & EATON, J. K. 1984 Experiments on the structure of a turbulent reattaching shear layer. Thermosciences Div., Dept of Mechanical Enging, Stanford University, CA., *Rep.* MD-43.

AMANO, R. S., GOEL, P. & CHAI, J. C. 1988 Turbulence energy and diffusion transport of third-moments in a separating and reattaching flow. *AIAA J.* **26**, 273–283.

BARKEY-WOLF, R. 1987 Swept and unswept separation bubbles. Ph.D. thesis, Cambridge University.

BRADSHAW, P. 1967 The turbulence structure of equilibrium boundary layers. *J. Fluid Mech.* **29**, 625–645.

BRADSHAW, P. & WONG, F. Y. F. 1972 Reattachment of a turbulent shear layer, *J. Fluid Mech.* **52**, 113–135.

CASTRO, I. P. 1973 A highly distorted turbulent free shear layer. Ph.D. thesis, Imperial College.

CASTRO, I. P. 1981 Measurements in shear layers separating from obstacles in rough wall boundary layers, *J. Wind Engng. Indust. Aero.* **7**, 253–272.

CASTRO, I. P. 1985 Time domain measurements in separated flows. *J. Fluid Mech.* **150**, 183–201.

CASTRO, I. P. & BRADSHAW, P. 1976 The turbulence structure of a highly distorted mixing layer. *J. Fluid Mech.* **73**, 265–304.

CASTRO, I. P. & CHEUN, B. S. 1982 The measurement of Reynolds stresses with a pulsed wire anemometer. *J. Fluid Mech.* **118**, 41–58.

CASTRO, I. P. & DIANAT, M. 1990 Pulsed wire anemometry near walls. *Expt. Fluids* **8**, 343–352.

CASTRO, I. P., DIANAT, M. & BRADBURY, L. J. S. 1987 The pulsed wire skin friction measurement technique. In *Turbulent Shear Flows V* (ed. F. Durst, B. E. Launder, J. L. Lumley, F. W. Schmidt & J. H. Whitelaw), pp. 278–290. Springer.

CASTRO, I. P., DIANAT, M. & HAQUE, A. 1988 Shear layers bounding separated regions. In *Turbulent Shear Flows VI* (ed. J.-C. André, J. Cousteix, F. Durst, B. E. Launder, F. W. Schmidt & J. H. Whitelaw) pp. 299–312. Springer.

CASTRO, I. P. & HAQUE, A. 1987 The structure of a turbulent shear layer bounding a separation region. *J. Fluid Mech.* **179**, 439–468 (referred to herein as CH).

CASTRO, I. P. & HAQUE, A. 1988 The structure of a turbulent shear layer bounding a separation region. Part 2. Effects of free-stream turbulence. *J. Fluid Mech.* **192**, 577–595.

CHANDRSUDA, C. & BRADSHAW, P. 1981 Turbulent structure of a reattaching mixing layer. *J. Fluid Mech.* **110**, 171–194.

CHERRY, N. J., HILLIER, R. & LATOUR, M. E. M. P. 1984 Unsteady measurements in a separated and reattaching flow. *J. Fluid Mech.* **144**, 13–46.

CHU, J. & YOUNG, A. D. 1976 Measurements in separating two-dimensional turbulent boundary layers. *AGARD CP*-168, Paper 13.

DENGEL, P. & FERNHOLZ, H. H. 1990 An experimental investigation of an incompressible turbulent boundary layer in the vicinity of separation, *J. Fluid Mech.* **212**, 615–636.

DEVENPORT, W. J. 1985 Separation bubbles at high Reynolds number: Measurement and computation. Ph.D thesis, Cambridge University.

DIANAT, M. & CASTRO, I. P. 1989 Measurements in separating boundary layers. *AIAA J.* **27**, 719–724.

DRIVER, D. M. & SEEGMILLER, H. L. 1985 Features of a reattaching turbulent shear layer in a diverging channel flow. *AIAA J.* **23**, 163–171.

EATON, J. K. & JOHNSTON, J. P. 1980 Turbulent flow reattachment: an experimental study of the flow and structure behind a backward facing step. *Rep.* MD-39. Thermo-Sciences Div., Dept Mech. Engng, Stanford University.

EATON, J. K. & JOHNSTON, J. P. 1982 Low frequency unsteadiness of a reattaching turbulent shear layer. In *Turbulent Shear Flows 3* (ed. L. J. S. Bradbury, F. Durst, B. E. Launder, F. W. Schmidt & J. H. Whitelaw), p. 162. Springer.

FOX, R. W. & KLINE, S. J. 1962 Flow regimes in curved subsonic diffusers. *Trans. ASME* D: *J. Basic Engng* **84**, 303–312.

JAROCH, M. 1985 Development and testing of pulsed wire probes for measuring fluctuating quantities in highly turbulent flows. *Expt Fluids* **3**, 315–322.

JAROCH, M. & FERNHOLZ, H. H. 1989 The three-dimensional character of a nominally two-dimensional separated turbulent shear layer. *J. Fluid Mech.* **205**, 523–552.

KAYS, W. M. & CRAWFORD, M. E. 1980 *Convective Heat and Mass Transfer*, pp. 178–179. McGraw-Hill.

KIYA, M. 1988 Separation bubbles. *Paper presented at the IUTAM Conference on Separated Flows, Grenoble.*

KIYA, M. & SASAKI, K. 1983 Structure of a turbulent separation bubble *J. Fluid Mech.* **137**, 83–113.

KIYA, M., SASAKI, K. & ARIE, M. 1982 Discrete-vortex simulation of a turbulent separation bubble. *J. Fluid Mech.* **120**, 219–244.

RODI, W. 1975 A review of experimental data of uniform density free turbulent boundary layers. In *Studies in Convection*, vol. 1 (ed. B. E. Launder). Academic.

RUDERICH, R. & FERNHOLZ, H. H. 1986 An experimental investigation of a turbulent shear flow with separation, reverse flow and reattachment. *J. Fluid Mech.* **163**, 283–322.

SHILOH, K., SHIVAPRASAD, B. G. & SIMPSON, R. L. 1981 The structure of a separating turbulent boundary layer. Part 3. Transverse velocity measurements. *J. Fluid Mech.* **113**, 75–90.

SIMPSON, R. L. 1983 A model for the backflow mean velocity profile. *AIAA J.* **21**, 142–143.

SIMPSON, R. L. 1985 Two-dimensional turbulent separated flow. *AGARDograph* 287.

SIMPSON, R. L., CHEW, Y. T. & SHIVAPRASAD, B. G. 1981*a* The structure of a separating turbulent boundary layer. Part 1. Mean flow and Reynolds stresses. *J. Fluid Mech.* **113**, 23–52.

SIMPSON, R. L., CHEW, Y. T. & SHIVAPRASAD, B. G. 1981*b* The structure of a separating turbulent boundary layer. Part 2. Higher-order turbulence results. *J. Fluid Mech.* **113**, 53–74.

SIMPSON, R. L., STRICKLAND, J. H. & BARR, P. W. 1977 Features of a separating turbulent boundary layer in the vicinity of separation. *J. Fluid Mech.* **79**, 553–594.

TOWNSEND, A. A. 1956 *The Structure of Turbulent Shear Flow*. Cambridge University Press.

WILLMARTH, W. W. & ROOS, F. W. 1965 Resolution and structure of the wall pressure field beneath a turbulent boundary layer. *J. Fluid Mech.* **22**, 81–94.

WOOD, D. H. & BRADSHAW, P. 1982 A turbulent mixing layer constrained by a solid surface. *J. Fluid Mech.* **182**, 57–89.

WOODWARD, D. S. 1970 An investigation of the flow in separation bubbles. Ph.D. thesis, Queen Mary College, London.